ALMA MATER STUDIORUM
UNIVERSITÀ DI BOLOGNA

DOTTORATO DI RICERCA IN

INGEGNERIA ENERGETICA NUCLEARE
E DEL CONTROLLO AMBIENTALE

ING-IND/10 Fisica Tecnica Industriale

XIX CICLO

MULTI-OBJECTIVE OPTIMIZATION OF MICROGAS TURBINE RECUPERATORS

Il Coordinatore del Corso di Dottorato
Chiar.mo Prof. Ing. Alessandro Cocchi

Il Relatore
Chiar.mo Prof. Ing. Enrico Nobile

Candidato Dott. Stefano Pieri

Trieste, 2007

..."I can see much clearer now, I'm blind"... [D.T.]

Dedicato ai miei pseudo-cugini acquisiti,
Lucy, Mattia e Valentino

Contents

List of Figures

V

Nomenclature

a	Plate corrugation amplitude [m]
A	Module heat exchange area, [m^2]
b	Channel height [m]
c_p	Specific heat [$J/(kgK)$]
f	Friction factor $f = \alpha 2b/(2\rho u^2)$
h	Local heat transfer coefficient [$W/(m^2K)$]
H	Module length in streamwise direction [m]
L	Wavelength of the corrugation [m]
ρ	Mass flow rate [kg/s]
$\mathbf{n}$	Unit vector normal to a surface
Nu	Nusselt number Nu $= h2b/\lambda$
p	Pressure [Pa]
Pr	Prandtl number Pr $= c_p\mu/\lambda$
Re	Reynolds number Re $= (\rho\bar{u}2b)/\mu$
T	Temperature [K]
u	Velocity in flow direction [m/s]
U	Global heat transfer coefficient [$W/(m^2K)$]
$\mathbf{W}$	Velocity vector [m/s]
x, y, z	Cartesian coordinates [m]
α	Overall pressure gradient in the flow direction [Pa/m]
β	Temperature gradient in the flow direction [K/m]
ϕ	Heat flux [W/m^2]
λ	Thermal conductivity [$W/(mK)$]
μ	Dynamic viscosity [$kg/(ms)$]
ρ	Density [kg/m^3]
θ	Included angle between corrugations [$degrees$]

Sub/Superscripts

b	Bulk
c	Cold
h	Hot
i	Inlet
o	Outlet
w	Wall
$\sim$	Periodic Component
$-$	Mean Value

Introduction

In the last few years, a clear trend to develop products faster, at competitive prices, and to a high quality standard has become evident in industry, following globalization and competitive markets. In order to meet these targets, computer-aided engineering tools started to be used in the design process. This tendence has been favored by the constant increase of the computational performances of available hardware, together with the decrease of their cost.

In particular, this topic has grown in interest in microgas turbines fields due to the possibility to produce low-cost combined heat and electrical power.

To achieve high efficiencies in small gas turbines, compact recuperators are mandatory to preheat air to higher temperature prior combustion, thus improving the overall cycle rendition. For this reason, efforts must be made to enhance the performances of these important heat exchangers.

In conventionally sized recuperators, complex, well designed fin configurations are used in order to improve the gas-air heat transfer. In order to avoid these costly and difficult to realize fin configurations, alternative recuperator designs are needed for microscale applications, capable to maximize the heat transfer coefficient as well as the compactness. Cross-corrugated primary surface heat exchanger is promising for this purpose.

Performance of such heat exchanger greatly depends on its plate geometry and shape, type of corrugation, corrugation pitch and corrugation angle, so a complete analysis of these relationships is needed during the design process.

It is on record that an engineering process can be considered as an iterative loop where new ideas are generated and evaluated on the base of the following five steps: analysis, synthesis, simulation, evaluation and decision making. If the performance of new design predicted by means of numerical models does not meet the objectives, it

is necessary to modify some parameters and evaluate again until satisfactory performance is obtained. This approach depends on the knowledge of the designer and in case of large number of variables and objectives it becomes unfortunately unfeasible. From these considerations, it is necessary to increase the level of automation adopting a numerical optimization technique to speed up the design process and to achieve better results.

Thus, the purpose of this thesis is to describe the organization, theoretical background and application of a novel methodology for the multi-objective optimization of both technical and economical aspects of microturbine recuperators by means of an automatic integration of different industrial design tools, i.e. computer-aided design (CAD), mesh generation tools and computation fluid dynamics solver, managed by a multi-objective optimization platform as schematized in Fig.1.

Obviously, a large amount of simulations is needed in order to evalutate the influence of all these geometrical variables. However it is possible and convenient to reduce the numerical analysis to one single periodic module, because this corrugated geometries are characterized by repetitive pattern in both streamwise and transverse directions. The temperature and the flow fields infact, become fully developed after a short entrance regime and repeat themself from module to module in a similar way. The core of this work consist in an integration of a commercial CFD solver, programming by means of the native command language, the appropriate periodic boundary conditions between inlet and outlet with a coupled conjugate approach, considering both hot and cold fluids and solid domains.

Regarding the objectives, high effectiveness must be achieved without detriment to pressure loss, that must be minimized due to its strong influence on gas turbine efficiency. These considerations are linked to economical aspects, which lay down serious constraints to the technically feasible solutions. The cost of the recuperator should not exceed the standard values, corresponding to the 25-30% of the whole micro turbine price.

All these technical and economical goals lead to a challenging design problems consisting of several conflicting objectives. Usually, the different objectives are combined into a mono-objective analysis, whilst in this thesis a more extensive approach has been adopted to face this optimization employing the Multi-Objective Genetic Algorithm (*MOGA*).

The result of such multi-objective optimization is a set of solutions - the so called Pareto Front - that displays the trade-off between the competing objectives; at the end of the optimization, different tools to analyze the results and to choose which of the solutions is the best have been utilized.

In summary, the present work reports the geometrical configuration and the param-
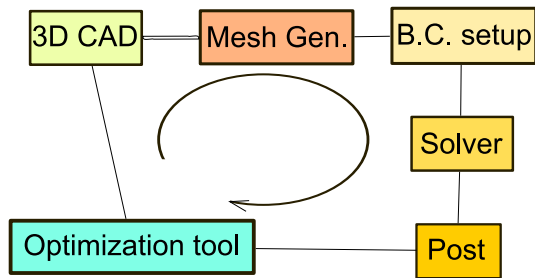
Figure 1   Automatic process chain.

eterization of the geometry of a compact heat exchanger, the definition and validation of the thermal and fluid-dynamics numerical model and finally the data analysis of the results of various optimizations of a $50kW$ microgas turbine recuperator obtained integrating all the different methodologies described above.

The final objective of the whole research is to find optimum configurations for high effectiveness and high compactness recuperators.

Chapter 1

Microgas turbine recuperators

1.1 Microgas turbine overview

Gas turbines can be arbitrarly categorized as "microturbines" ($5 - 200\,kW$) and "miniturbines" ($200 - 500\,kW$). The main difference between small and large gas turbines is the amount of gas involved into an almost unchanged thermodynamic cycle. Velocity and pressure levels remain the same when scaling down a gas turbine, even if the dimensions are smaller. The work exchange between compressor or turbine and fluid is proportional to the peripheral speed, such that the rotational speed should scale inversely proportional to the diameter, resulting in speeds of more than $500000\,rpm$ for rotor diameters below $20\,mm$.

A major problem with the miniaturization of microturbines is a large decrease in Reynolds number, resulting in higher viscous losses and a lower overall cycle efficiency. Also the required temperature is a problem, in fact, since a pressure ratio of 3 is expected, the turbine inlet temperature should be at least $1200\,K$ to obtain a positive cycle efficiency, thus higher temperatures would considerably boost the overall efficiency. In large turbines, the blades are cooled by internal cooling channels and protected by thermal barrier coatings, whilst in case of microturbines, internal cooling of such small blades is unrealistic, therefore temperatures of $1200\,K$ and higher can only be reached with ceramic materials.

Another major consequence of the small dimensions is the extreme temperature gradient between the hot turbine and colder compressor. The resulting massive heat flux causes a non-negligible decrease of both compressor and turbine efficiency. Given that gas turbine net power output is the small difference between the turbine power output and the compressor energy requirements, the deterioration of aero-performance of the components with decreasing dimensions and increased heat transfer, results in an even larger decrease of power output and cycle efficiency.

The simpliest microgas turbine (MGT) system can be schematized as shown in Fig.1.1, where three components are connected in order to define the temperature-

entropy Brayton chart indicated in Fig.1.2: a compressor, a combustion chamber and a turbine. Even though these three devices are sufficient, however a recuperator is needed to achieve desirable system thermodynamic efficiency. In this section, a brief description of the general features of a gas turbine, the main governing equations and the different phases of the ideal Brayton cycle are given.
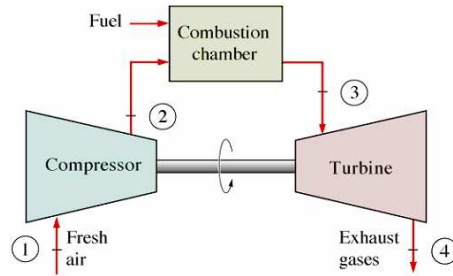
Figure 1.1   An open ideal Brayton cycle.
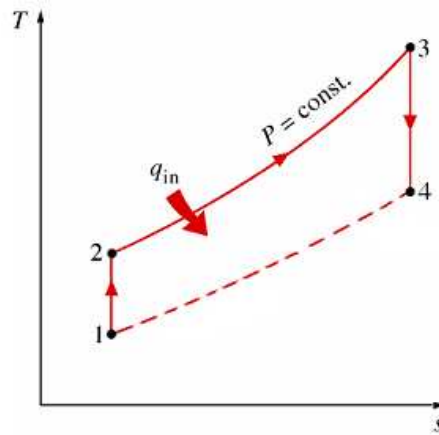
Figure 1.2   Ideal Brayton cycle, T-s diagram.

The system in Fig.1.1 is an open cycle, because there are mass flows in (fresh air) and out (exaust gases) of the process. At stage 1, the compressor increases the pressure of the fresh air on the base of its size and construction; during compression, the

pressure and temperature increase even though the entropy is constant. At stage 2 the high-pressure air and fuel are mixed and burnt in the combustion chamber at a constant pressure where density decreases and specific volume and temperature increase. Next, the hot gas enters the turbine at stage 3 and forces the turbine to rotate producing mechanical work, thus the turbine behavior is the opposite than the compressor, in fact the pressure decreases and specific volume increases. In the open cycle, at stage 4 the exhaust gases are released to the surroundings. Since the efficiency of the gas turbine is the ratio of produced net work and added heat power, it can be written as:

$$\eta_{id} = \frac{w_{net}}{q_{in}} = 1 - \left(\frac{q_{out}}{q_{in}}\right) = 1 - \left(\frac{T_4 - T_1}{T_3 - T_2}\right) \tag{1.1}$$

We can relate the temperatures to the pressures with the isentropic relations:

$$\frac{T_2}{T_1} = \left(\frac{P_2}{P_1}\right)^{(k-1)/k} \quad ; \quad \frac{T_3}{T_4} = \left(\frac{P_3}{P_4}\right)^{(k-1)/k} \tag{1.2}$$

Since that $P_2/P_1 = P_3/P_4$, the efficiency can be rewritten as:

$$\eta_{id} = 1 - r_p^{(1-k)/k} \tag{1.3}$$

where r_p represents the pressure ratio. From Eq.(1.1) it is possible to deduce that the higher pressure ratio of the gas turbine, the higher is its efficiency. The equation is valid only for ideal gas turbines with no friction and reversible processes.
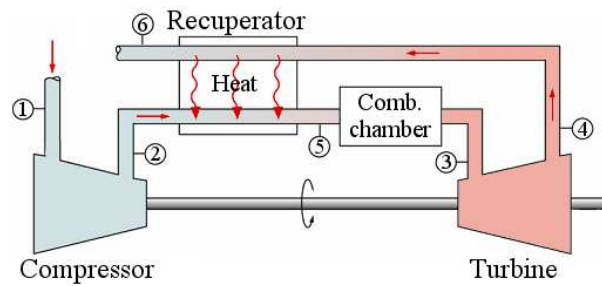
Figure 1.3   An open ideal Brayton cycle with recuperator.

Large gains could be made if the heat of the exhaust gases leaving the turbine could be reused, instead of being rejected to the surroundings and this can be obtain with a recuperator. As shown in Fig.1.3 the hot exhaust gas can preheat the fresh air
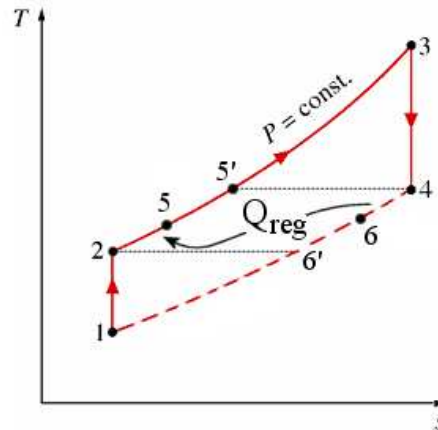
Figure 1.4   Ideal Brayton cycle with recuperator, T-s diagram.

going into the combustion chamber, thus reducing the fuel requirements for the same net work output. The corresponding $T - s$ diagram is indicated in Fig.1.4.

In practice, to allow heat transfer, the temperature of the air leaving the recuperator at state 5 must be less than the temperature at state 4 and, in the same way, the temperature at state 6 must be higher than the temperature at state 2. Points 5′ and 6′ correspond to the extreme points using a ideal counter corrent heat exchanger. The efficiency of a conventional recuperative cycle can be written as:

$$\eta = \frac{w_{net}}{q_{in}} = 1 - \left(\frac{q_{out}}{q_{in}}\right) = 1 - \left(\frac{T_{6'} - T_1}{T_3 - T_{5'}}\right) = 1 - \left(\frac{T_1}{T_3}\right)r_p^{(k-1)/k} \tag{1.4}$$

where T_1 and T_3 are the temperatures before compression (the ambient temperature) and after combustion respectively. Therefore, for an ideal Brayton cycle within recuperator, the thermal efficiency depends not only on the pressure ratio, but also on the temperature ratio. Moreover, the equation shows that the higher difference between the temperature at which heat addition (combustion) and heat rejection (exhaust gas leaves and fresh air comes in) occurs, the higher is the efficiency. A most important aspect to notice is that, on contrary to a simple Brayton cycle, the thermal efficiency of a Brayton cycle with recuperator decreases with the increase in pressure ratio. This correlation is better explained in Fig.1.5 where r_p^* is the intersection point between the curve of the simple Brayton and the curve of the cycle within recuperator

in case of temperature ratio equal to 0.3. If the pressure ratio of the system is higher than r_p^* the simple cycle has higher effectivness and vice versa.

A recuperator with a higher efficiency will obviously save a greater amount of fuel since it will preheat the air to a higher temperature prior combustion. In larger gas turbines there are additional possible stages, as for example intercooling and two stage expansion and compression. These stages will increase the total efficiency, but will make the gas turbine more expensive to manufacture and more complex.
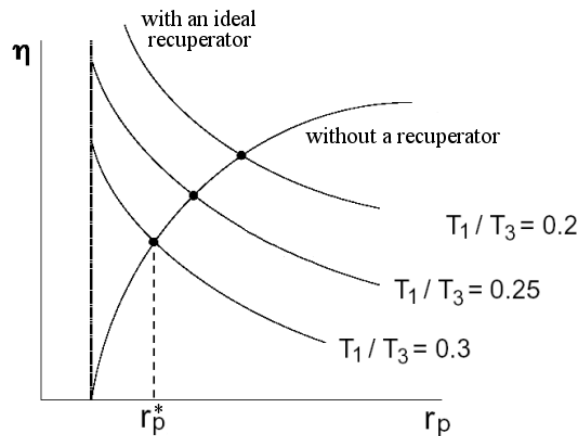
Figure 1.5   Effect of pressure and temperature ratios on thermal efficiency.

1.2   Recuperators

As explained previously, recuperators are essential devices to obtain high performances and elevated renditions in small gas turbines. In a state of the art machine, in which the temperature of the gas at the turbine inlet is around 1200 K, the efficiency can reach values of $28 \div 30\%$, about ten points higher than a non regenerative cycle. The U.S. Department of Energy has promoted the Advanced Microturbine System Project to develop the advanced technologies needed to realize regenerative microgas turbines having efficiency values up to $40 \div 45\%$, cost lower than $500\$/kW$ and NOx emissions lower than 10 ppm, able to be fed with various fuels and to operate without significant maintenance for time intervals of a few years [2]. Moreover, it is well

known that with further developments efficiency could reach 50% [3].

The reaching of the just pointed out performance goals depends significantly on the possibility of being able to design and realize recuperators with advanced characteristics from the viewpoint of thermo fluid-dynamics effectiveness, mechanical strength at high temperatures and manufacturing costs.

As far as the thermal fluid dynamics aspects are concerned, actual cycle efficiency values can be obtained with recuperators having effectiveness values equal to or higher than 85% [4]. An effectiveness increase of 1% gives a gas turbine efficiency improvement of about 0.35 points [4]. Effectiveness values of 90% and higher are usually considered today: unfortunately, starting from so high values, every further increase involves a dramatic growth of the heat transfer surface. For example, going from 90% to 95% the recuperator core dimensions double and they double again if effectiveness has to reach 97.5% [3]. So it is evident that the requested cycle efficiency and recuperator effectiveness improvements can be practically obtained only looking for innovative design solutions, capable to maximize the heat transfer coefficient as well as the compactness and lightness of the whole recuperator.

As far as dimensions are concerned, microgas turbine applications require small values for both the cross sectional area of the flow channels, which means small values of the hydraulic diameter, and the metal sheet thickness. Hydraulic diameter (D_i) is the design variable which probably has the greatest impact on the recuperator core volume. A small diameter gives a small volume, but too reduced values could be unacceptably sensitive to fouling and too expensive to fabricate. Values of D_i around one or two millimeters could be considered as a trade-off among the described technical constraints. Metal sheet thickness is an important design variable: because thermal and mechanical stresses must be taken into account, together with the commercial availability, values around $0.05 \div 0.08$ millimeters can practically be considered.

Unfortunately high effectiveness is directly connetcted to pressure loss, which must be minimized due to its strong influence on gas turbine efficiency. Actually, a loss reduction of 1% brings an improvement in gas turbine efficiency of about 0.33% [4], thanks to the better use of the power taken by the compressor and to the control of the counter pressure which interferes with the gas flow rate in the turbine wheel. That is the reason why the fluid-dynamics of the flow channels and of the air and exhaust gas ducts must be carefully studied in order to maintain the total pressure drop under the value of $4 \div 5\%$.

As far as the mechanical aspects are concerned, materials must be chosen suitable to withstand the more and more higher thermal stresses which result from the expected increase, in the small turbine field also, of the combustor mean temperature. Until temperature of 950 *K* austenitic stainless steel of the 300 series can be used [5], while

with higher temperatures, alloys less subject to creep distortion and corrosion must be utilized [6]. The material choice process must also take into account the requirement of assuring to the device an in service life of about 60.000 hours, with some thousands starting and stopping operations which cause strong thermal stresses [4].

The mechanical strength is an important issue because recuperators are manufactured with extremely thin metal sheets, so creeps can cause the dilatation of the compressed air channels provoking a counter pressure increase due to the narrowing of the exhaust gas passages. As a whole, the distortions can cause significant variations of the heat transfer surfaces geometry [7].

This considerations are linked to economical aspects, which lay down serious constraints to the technically feasible solutions. The cost of the recuperator should not exceed the standard values reported in the recent literature, corresponding to the $25 \div 30\%$ of the whole micro turbine price [8]. If the effectiveness rises from 85% to 90%, the recuperator cost normally increases of 50% [9]. Moreover, the cost of the core represents the $50 \div 75\%$ of the whole recuperator cost, and it can be valued in 1.5 times the cost of the material for highly corrosion and creep resistant alloys [10] and $3.5 \div 4$ times for the 347 stainless steel [11].

1.3 Recuperators classification

In the previous section the basic concept of *MGT*-cycle and the importance of using recuperators have been discussed. This is the purpose why efforts must be made to design compact and low cost heat exchangers, able to minimize pressure drops and maximize effectiveness. To such extent, new design concepts have been proposed, as the spiral recuperator presented by Acte S.A. [12] or Rolls-Royce (Fig.1.7) or the multiple concentric tube *PROE*90*TM* shown in Fig.1.6 [13]. The basic element of the this recuperator is a concentric tube assembly that, in the preferred embodiment, is comprised of four concentric tubes that enclose three concentric annular flow passages. The low pressure exhaust gas flows through the inner and outer annular passages while the high pressure compressor exit air flows through the annular passage that is between the two low pressure passages. The high and low pressure flows are in opposite directions to achieve the high effectiveness that is only available with a counterflow heat exchanger. Heat is transferred from the exhaust gas to the compressor air though the tube walls on each side of the high pressure channels.

Figure 1.6 PROE 90TM (Courtesy of Proe Power Systems, LLC).
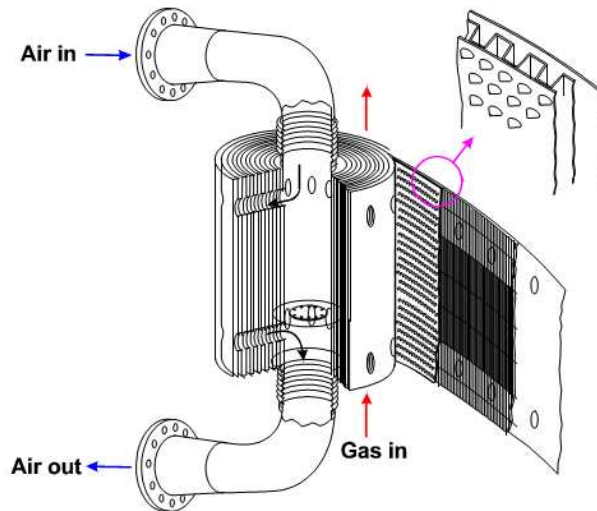
Figure 1.7 Spiral heat exchanger (courtesy of Rolls-Royce).

This kind of devices may be fulfilled with more traditional, easier to manufacture and cheaper compact recuperators. The traditional compact heat exchanger geometries can be classified according to transfer process, constructon, flow arrangement, surface compactness, number of fluids or heat transfer mechanisms. Next is provided a brief description of the four main types of traditional exchangers classified according to construction: shell-and-tube, tube-fin, plate-fin, and primary surface recuperators.

1.3.1 Shell-and-tube

The tubular exchangers are widely used because of the large range of operating conditions, such as from vacuum to ultra-high pressure, from cryogenics to high temperatures, and because of the allowed differences of fluids properties, i.e. temperature and pressure, limited only by the material of construction. Shell-and-tube recuperators can be designed for special operating conditions as vibration, heavy fouling, erosion, corrosion, toxicity and so on. They are the most versatile exchangers made from a variety of metal and non-metal materials and in sizes from 0.1 m^2 to over 100000 m^2. They are basically non-compact exchangers and consist of a series of tubes within an outer shell. One fluid flows through the tubes while a second fluid flows between the outer shell and the tubes, exchanging heat from one fluid to the other. They have been used for decades in the process industry and in large gas turbines. Consequently, knowledge is extensive about their design, construction, and operation. However, because shell-and-tube recuperators are typically very large and bulky, they are not normally used on microturbines.

1.3.2 Tube-fin type

In this type of exchangers, round, rectangular and although elliptical tubes are coupled with external or internal fins. They are attached to the tubes in several ways such as by a tight mechanical fit, adhesive bounding, soldering, brazing, welding or extrusion. Depending upon the fin type, the tube-fin exchangers are subdivided into three gruoups:

- *finned tube exchangers* as shown in Fig.1.8, having normal fins on individual tubes;

- *tube-fin exchanger having flat and continuous fins*; they can be plain, wavy or interrupted, and the array of tubes can be circular, oval, rectangular or other shapes as shown in Fig.1.9;

- *longitudinal fins* on individual tubes generally used in condensing applications
  and for viscous fluids in double pipe heat exchangers.
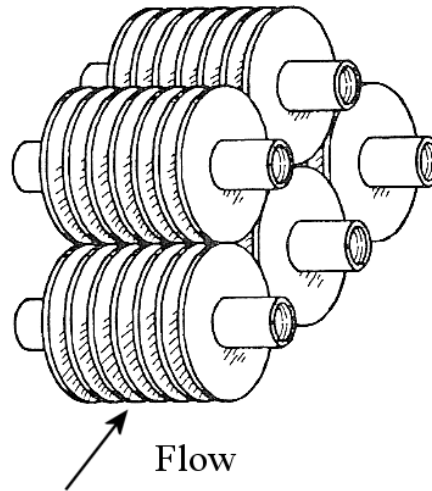
Figure 1.8   Individually finned tubes.

Tube-fin exchangers can support high pressure on the tube side, and the highest
temperature is limited by the type of bonding, materials and thickness. These exchangers are used as condensers and evaporators in air-conditioning and refrigeration
applications.

1.3.3   Plate-fin type

Plate-fin heat exchangers consist of finned chambers separated by flat plates that route
fluid through alternating hot and cold passages. Heat is transferred via fins in the
passageways, through the separator plate, and into the cold fluids via fin once again.
One of the many plate-fin types, called *offset strip fin* (or *staggered fin*), is shown in
Fig.1.10. The efficiency of thermal transport to the separating metal sheets of the fins,
depends on their height, material conductivity etc. The fins could often be brazed
to the separating metal sheets to secure a good thermal contact. This configuration
results in a higher mass of the recuperator unit and moreover only a fraction of about

Flow
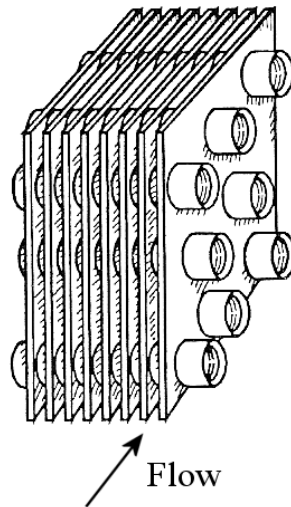
Figure 1.9 Continuous fins on an array tubes.

$75 \div 80\%$ of its surface is effective to heat transfer purposes [10], so the plate-fin type could be not convenient.

1.3.4 Primary surface

Primary surface recuperators consist of folded thin metal foils or plates packed together. Generally, these exchangeers could not support very high pressures, temperatures and temperature gradients. The shapes of the plates can vary significantly so they can be mainly categorized in: *cross-corrugated*, *corrugated-undulated* and *cross-wavy*. It can be assumed that recuperators based on these kind of primary surfaces are able to decrease the volume and the material weight by 50% or more, when compared to an equivalent plate-fin heat exchanger [10].

Cross-corrugated recuperators (*CC*) are obtained packaging identical corrugated metal sheets alternating the extrusion angle compared to the main axial direction as shown in Fig.1.11. The main geometrical characteristics are P, which is the wavelength between two peaks, H and H_i, respectively the external and internal height of the half channel, and the wall thickness s, which is given by the difference between H and H_i. Moreover, for this kind of recuperators, the quantity of material, which means
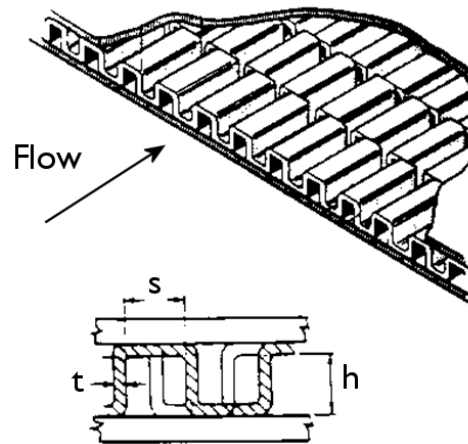
Figure 1.10   The offset strip-fin surface.

its weight, is the main parameter that affects the final cost.
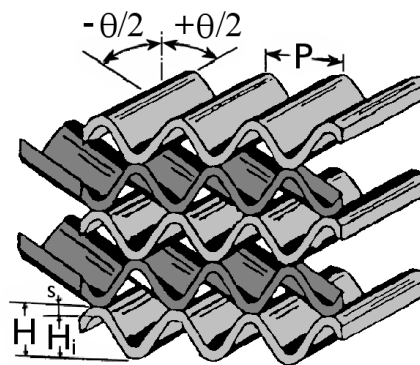
Figure 1.11   Cross-Corrugated recuperator.

Concerning the cross-undulated geometry (CU) shown in Fig.1.12, it is a variation of the cross-corrugated geometry, in which the shapes of the surfaces have two different corrugation profiles and the gas-air interfaces are alternately subdivided by planar

metal sheets. The reason of this choice is that the hot and cold fluids have different physical properties and pressure so providing a larger cross-area for low pressure flow, leads to minimize the pressure drop of the low density exhaust gases.

Cross-undulated surfaces have been recently considered in rotary air pre-heaters studies [14], but the main limit in their use is a lack of knowledge in how performance is impacted by the geometrical variables [15].

The cross-wavy recuperator (*CW*) illustrated in Fig.1.13, is a commercially available primary surface concept, in which the waviness in the main flow direction of the upper and lower duct halves is 180 degrees out of phase relative to each other, thus forming the fluid domains. The wavy corrugation of this wavy surface is obtained using a folding process because pressing or stamping the sheets is not possible due to the very small pitch and relatively high height of the passage.

Cross-corrugated and cross-wavy surfaces have both good performances, but the first ones are easier to manufacture and better documented in literature than cross-wavy ones.

1.4 Literature review

In literature, many case of experimental and numerical analysis of complex heat transfer surfaces is treated. A detailed description of the three papers that mainly affected the choice of the geometry to analyze in this thesis is given below.

G.Croce, P.D'Agaro

In this work [16], the cross-corrugated geometry has been chosen to carry out a three-dimensional investigation of flow and heat transfer. The nature of the fluid is intrinsically three-dimensional, thus a detailed description of the whole flow field is impossible to obtain by analytical investigations and very difficult to reach experimentally. Thereby the authors claim that numerical analysis is a very convenient tool to get complete behavior of the complex flow structures over the domain.

Since the corrugation geometry is correlated to the thermo fluid-dynamic perfomance of the recuperator, a large variety of corrugated profiles has been investigated for many different cross-sections. At least they have focused on sinusoidal corrugation with a 90° angle between adjacent plates.

This corrugated ducts are characterized by repetitive geometry in both streamwise and transverse directions. The temperature and the flow fields become fully developed after a short entrance regime and repeat themself from module to module in a similar
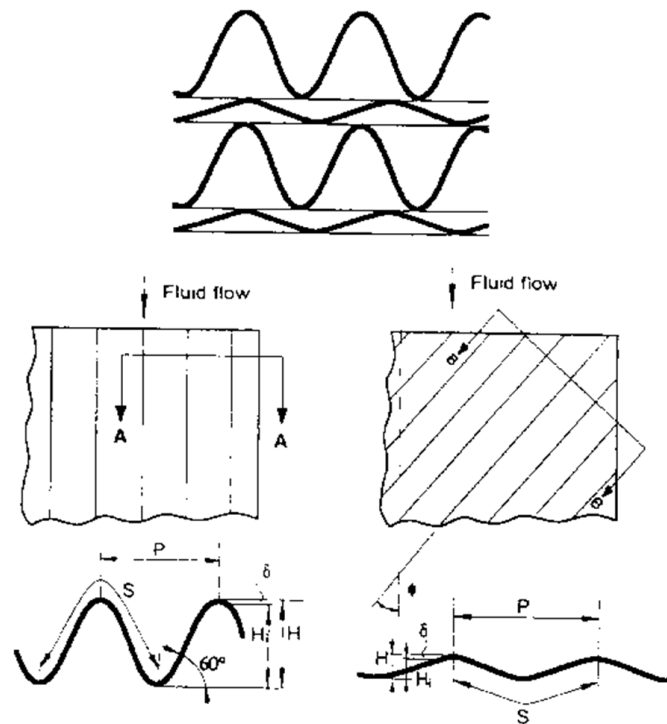
Figure 1.12 Corrugated-Undulated recuperator.

way. Because of that, it can be possible and convenient to reduce the numerical analysis to this single periodic module. From a thermal point of view, uniform temperature condition is assumed on the heat exchange walls while the periodicity of thermal field between inlet and outlet is imposed. The authors have been performed calculations for six Reynolds numbers ranging from 10 to 1000. They observed two different flow regimes: steady flow for $Re < 300$ and unsteady behaviour for $Re > 300$. For higher Re in fact, the flow solution becomes time dependent and self-sustained oscillations in the flow quickly lead to semi-chotic phenomena.
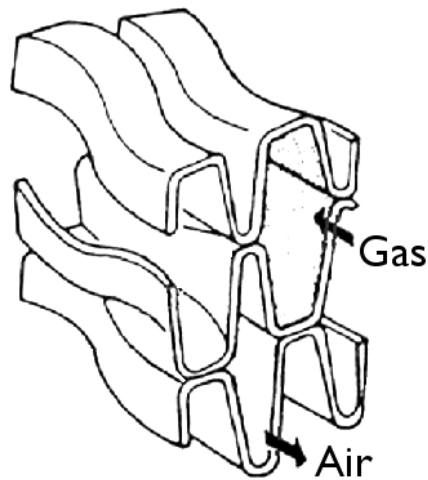
Figure 1.13 Cross-Wavy recuperator.

Stasiek J., Collins M. W., Ciofalo M.

In [1, 17], an experimental and numerical study of flow and heat transfer has been conducted for a cross-corrugated geometry. By means of a finite volume method, a variety of approaches ranging from laminar flow to k-ϵ turbulence model, direct numerical simulation and large eddy simulation were obtained.

Figure 1.14 shows the computational domain of the heat exchange matrix, which was used in the numerical simulation. Many computational results are presented in the paper for mid plane and the two sections $C - C$ and $N - N$ whitin a range of $Re = 10^3 \div 10^4$ and cross-angles θ betweeen $30°$ and $150°$. As regards thermal boundary conditions, the authors remark that the ones closest to those prevailing in real air heat exchangers are uniform wall temperature conditions, which were thus adopted in most runs. Uniform wall heat flux conditions were also tested, and gave slightly larger values of the mean heat transfer coefficients. Finally, in order to draw comparisons of the results with experimental data, they carried out a third kind of thermal boundary conditions: the bottom wall was assumed to be adiabatic while on the opposite wall the following condition was imposed: $q_w = (T_b - T_w)/R$. This simulates the experimental conditions, represented in Fig.1.15 where T_b is the constant temperature of the water
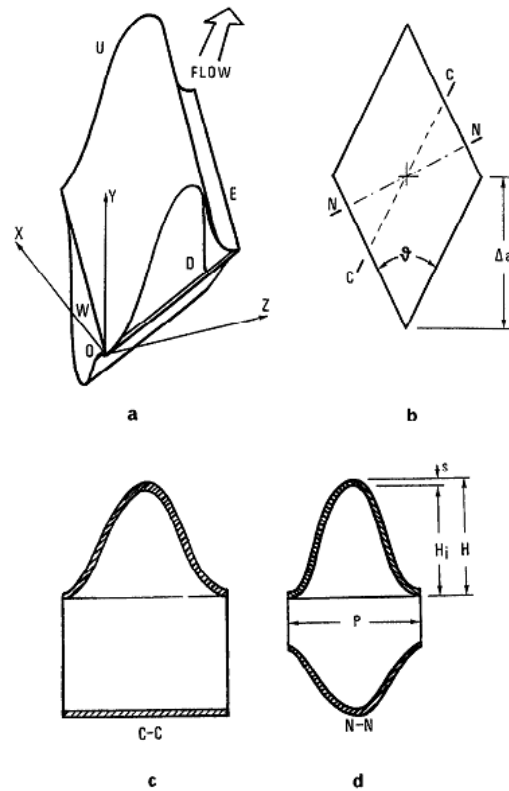
Figure 1.14 Unitary cell: (a) Perspective view; (b) section with midplane $y = 0$; (c) $C - C$ section; (d) $N - N$ section.

bath cooling the outer side of the top corrugated plate and R is the thermal resistance of the plate and liquid crystal package.

Blomerius H., Mitra N.K.

In [18], flow field and heat transfer in cross-corrugated ducts have been investigated by means of CFD simulations in the laminar to transitional range of Reynolds numbers as in [16]. Geometries with different cross-angles given by the corrugations and the main stream direction, between 45° and 90° have been considered because, as they report,
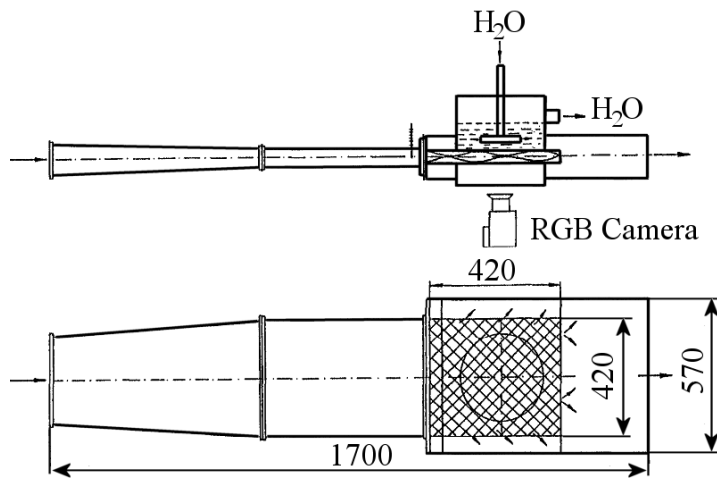
Figure 1.15 Setup of the device for the experimental analysis, [1].

the overall heat transfer and pressure drop depend strongly on this angle. As in the other works, a periodic element of the duct is chosen to be the computational domain, and periodic boundary conditions are assumed at the entrance, the exit and at the sides whilst uniform temperature condition is assumed on the heat exchange surfaces. The results presented by the authors strongly agree with the behavior of the similar paper found in literature, confirming the possility to focus the numerical simulation on a single cross-corrugated module by imposing proper periodic boundary conditions.

Chapter 2

Geometry parameterization

2.1 Introduction

In the previous chapter, the choice of the cross-corrugated shape as the best geometry to get the purposes of this thesis has been done considering the simplicity of the manufacturing and the availability of the data in literature needed for the validation of the numerical results.

Because of the optimization process which is intent to be done, a large number of CFD simulations is needed to be evaluated, and as a consequence, a large number of different geometries is needed to be generated. To reduce the time necessary to generate all these models, a semi-automated approach needs to be applicated, which means that the geometry has to be built just once and for all, so that some geometric entities like edge lenghts or point coordinates, defined as parameters from the outside, could vary the overall shape or size of the domain.

2.2 Parameterization overview

The research in parametric design was born approximately in 1960s, in which the idea of using geometric constraints to modify graphics was presented. Since then, parametric design had a quick developing history. The concept of "feature" which was presented in 1980s and developed in the next years [19], laid down the foundation of parametric design. In that years, *Parametric Technology Corp.* covered the market with its new generation solid modeling software, *ProEngineer* [20], which is based on parametric, variational and feature design, whilst *Premise Corp* was developing the commercial software *Designview*. In [21] firstly the concept of "variational geometry" has been presented, in which parametric design was researched further. Up to now, many parametric design methods, such as variants programming, knowledge-based parametric design, variational geometry and variational design, history-based

constraint modeling or parametric feature-based design, [22] appeared.

Accompanying the growth of parametric design theory, the CAD software has also had an extraordinary development. The early CAD systems could only treat two-dimensional drawing by simply connecting the basic geometrical elements, such as point, line, circle, arc, etc. and the result was just the visual graphics, which did not comprise the topological relationships and dimension constraints between different parts of the product. Therefore, when some details of the graphics need to be modified, the drawing has to be redrawn entirely, which makes the designer waste lots of time in repeating the monotonous similar operations. The typical system of this kind of software is *AutoCAD*. With the development of computer technology, the three-dimensional functions, such as 3D modeling, virtual assembly, dynamics simulation, and interference verification can be easily realized in current computer. Developing from *Brep* (Boundary Representation), *CSG* (Conshuctive Solid Geometry) and *hybrid model* to feature modeling, the 3D functions of the CAD software become more and more powerful and sophisticated. The typical contemporaneous 3D CAD systems are *I-DEAS*, *ProE*, *CATIA*, *Solidworks*, and so on. Therefore the parametric design plays a more and more important role because it can accelerate the development process of product, shorten the design and manufacture cycle of product, improve product quality, reduce cost, and enhance the capacity of market competition and originality innovation.

2.3   Parametric curves

In order to parameterize a simple geometrical entity, it is necessary to define in parametric way its basic properites, e.g. the coordinates of a point or the length of a line. The higher is the complexity of the geometry the higher is the number of parameters. For example, to parameterize a circle, it is possible to choose one of the following groups of parameters:

- the coordinates of the center and the radius,

- the coordinates of the center and one point belonging to the circle,

- the coordinates of two points of the circle and the radius,

- the coordinates of three points,

- the bitangent and the radius,

- the tritangent,

- the coordinates of the center and one tangent.

Nevertheless, usually happens that the model has complex $3D$ curvilinear edges, so it is possible to choose between many different methods to parameterize the geometry. The more adopted methodologies to parameterize a curve are the spline and the Bazier curves. The detail of the theory behind these two methods are given below.

2.3.1 Spline curves

Parametric equations can be used to generate curves that are more general than explicit equations of the form $y = f(x)$. A typical quadratic parametric spline may be written as:

$$\mathbf{P} = \mathbf{a_2}t^2 + \mathbf{a_1}t + \mathbf{a_0} \tag{2.1}$$

where $\mathbf{P}$ is the point we are trying to find, $\mathbf{a_0}$, $\mathbf{a_1}$ and $\mathbf{a_2}$ are three vectors defining the curve and t is a parameter in a range between 0 and 1. In order to solve this equation, three points on the curve, labelled $\mathbf{P_0}$, $\mathbf{P_1}$ and $\mathbf{P_2}$ have to be specified; these are the positions along the curve given by the relevant parameter t. By convention, two of the selected points are the ends of the curve. By substituting the values into the equation, as a result we obtain a system of three equations:

$$\begin{cases} \mathbf{P_0} = \mathbf{a_0} & t = 0 \\ \mathbf{P_2} = \mathbf{a_2} + \mathbf{a_1} + \mathbf{a_0} & t = 1 \\ \mathbf{P_1} = \mathbf{a_2}t_0{}^2 + \mathbf{a_1}t_0 + \mathbf{a_0} & t = t_0 \end{cases} \tag{2.2}$$

and by solving these it is possible to find $\mathbf{a_0}$, $\mathbf{a_1}$ and $\mathbf{a_2}$ in terms of $\mathbf{P_0}$, $\mathbf{P_1}$ and $\mathbf{P_2}$:

$$\begin{cases} \mathbf{a_0} = \mathbf{P_0} \\ \mathbf{a_1} = \mathbf{P_2} - \mathbf{P_0} - \mathbf{a_2} \\ \mathbf{a_2} = ((\mathbf{P_1} - \mathbf{P_0}) - t_0(\mathbf{P_2} - \mathbf{P_0})) / t_0(1 - t_0) \end{cases} \tag{2.3}$$

An example is given in Fig.2.1, where a spline obtained with the set of values reported in Tab.2.1 is shown. The values of the coefficients obtained solving the system of equation for this case are $a_2 = (-1.25, 0.833)$, $a_1 = (3.25, 0.167)$ and $a_0 = (0, 0)$.

Although this method employed to create curves is easy to use, it is not immediately clear how these shapes come about. The curve is actually a combination of two quadratic curves, one is $y = f(t)$ and one is $x = f(t)$. By varying t between 0 and 1 as already written, x and y will both vary and create the curve, as indicated in Fig.2.2, where a coupled graphic method to build the curve is illustrated. The intersection between the projections of $x(t)$ and $y(t)$ gives the point belonging to the curve.

x_0	y_0	t_0	x_1	y_1	t_1	x_2	y_2	t_2
0	0	0	1.1	0.2	0.4	2	1	1

Table 2.1   Table of the Spline coefficients.
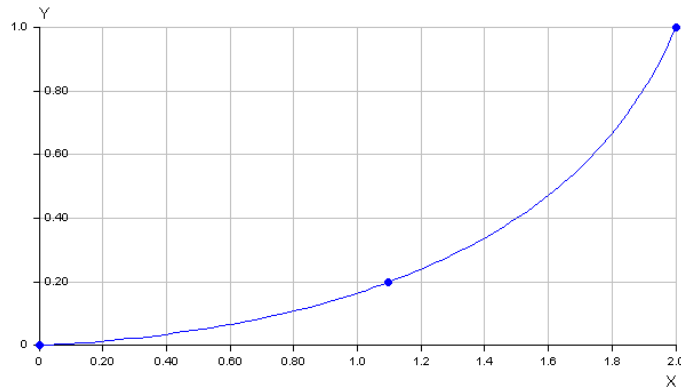
Figure 2.1   Chart of Spline.

2.3.2   Bezier curves

In §2.3.1, curves defined wholly in terms of the points through which they pass have been considered. This is a logical way of thinking, though it could suffer from drawbacks, infact, to make arbitrarily complex curves using just one equation, leads to higher degrees of polynomial and this make the problem mathematically awkward. One solution is to create complex curves merging many simpler curves called *patches*, however it is not acceptable to match just the end points, because it is necessary to match gradients as well. Defining curves by the points through which they pass does not lend itself very well to patching, thus a different approach based on the so called Bezier curves is needed.

The most commonly used Bezier curves of third order are fully defined by four points, known as knots. Two of these are the end points of the curve, while the other two effectively define the gradient at the end points. These two points control the shape of the curve so it is actually a blend of the knots as usually happens in an approximation of curves.

From a wide point of view, a n-order Bezier curve is a smooth curve defined by the x_k and y_k coordinates of its control points as indicated in formula 2.3.2, where n is
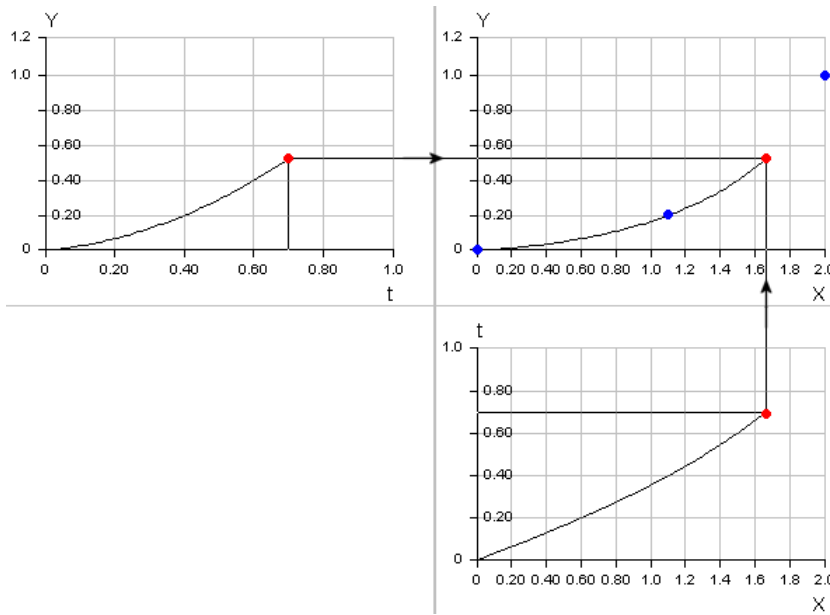
Figure 2.2 Graphic method to build a Spline.
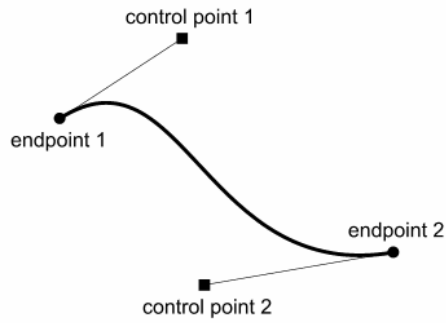
Figure 2.3 Third order Bezier curve.

the degree of the curve ($n + 1$ represents the number of the control points), and t is a number beween 0 and 1.

$$
\begin{cases}
x(t) = \displaystyle\sum_{k=0}^{n} \frac{n!}{k!(n-k)!} t^k (1-t)^{n-k} x_k \\[2ex]
y(t) = \displaystyle\sum_{k=0}^{n} \frac{n!}{k!(n-k)!} t^k (1-t)^{n-k} y_k
\end{cases}
\tag{2.4}
$$

An even simpler explanation about the Bezier curve algorithm should be given by a geometrical point of view: as shown in Fig.2.4, the sides of the control polygon are divided in manner that all of the two segments of this lines stay in the relation $t_0 : (1 - t_0)$. The points obtained in this way and thus connected by straight lines, are divided adopting the same proceeding until the reaching of point $p(t_0)$. It is possible to notice that $p(t_0)$ is the tangent point between the last line and the Bezier curve, so locally each line throught each $p(t)$ is tangent to the curve in that point. Therefore Bezier curves are very useful to get control over curvature at the ends and to carry out complex curves even with a small number of parameters.
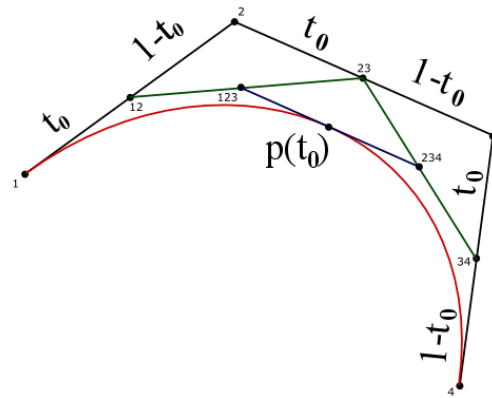
Figure 2.4   The construction of the Bezier curve.

2.4   Primary surface parameterization

The two main methods to parameterize complex curved geometries have been just presented. To build the geometry of the cross-corrugated primary surfaces of the compact

heat exchanger, the commercial parametric CAD software *CATIA* has been utilized adopting the Bezier curve approach, following the process explained below. First of all it is necessary to define the main curve of the corrugation by means of the seven points indicated in Fig.2.5. This main curve is made in fact by two Bezier curves of third order (the so called *patches*) defined each by 4 control points, the first having points from 1 to 4 and the second one from 4 to 7. To guarantee the same tangent of this two curves, points 1,2,6,7 and 3,4,5 are alingned on two parallel axes.
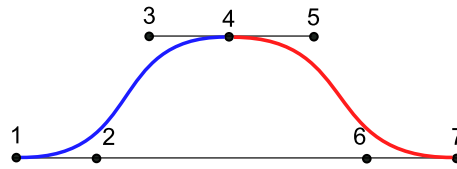
Figure 2.5 Bezier curves.

In this way, it is possible to define four parameters as follows:

$$P1 = x_2 - x_1; \quad P2 = x_4 - x_3; \quad P3 = x_5 - x_4; \quad P4 = x_7 - x_6. \tag{2.5}$$

These lenghts define the Bezier curves in parametric way, which means that changing these values it gives, as result, a new main shape of the curve that will constitute the geometry of the half flow cross-section area. In Fig.2.6 a possible configuration is shown, for example, doubling $P3$, halving $P2$ and keeping constant the others two parameters.
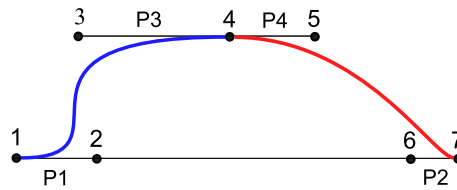
Figure 2.6 New Bezier curves obtained modifing $P2$ and $P3$.

Once the main curve has been generated and parameterized, it is possible to obtain the first corrugated surface laying on the bottom by copying it several times and then extruding it in the direction shown in Fig.2.7, forming an angle equal to $+\theta/2$ compared to the main flow direction indicated with the dash-dotted line.
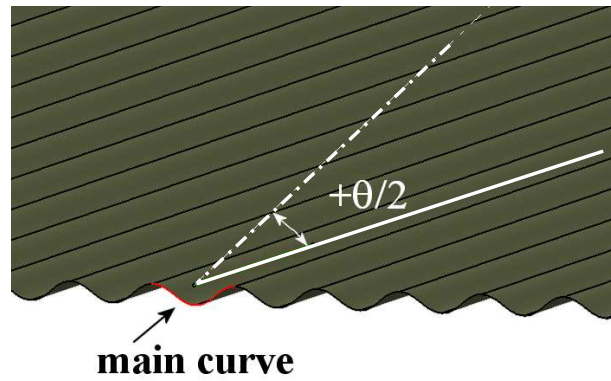
Figure 2.7 Costruction of the first corrugated surface on the bottom.

To get the first fluid domain, the main curve needs to be put on top of the just created surface, shifted by a half wavelenght $\lambda/2$ and then extruded in the direction forming the angle equal to $-\theta/2$, as shown in Fig.2.8. The angle θ has been chosen as one of the parameters for the optimization because of its elevated influence on the thermal and fluid-dynamics behavior [18].
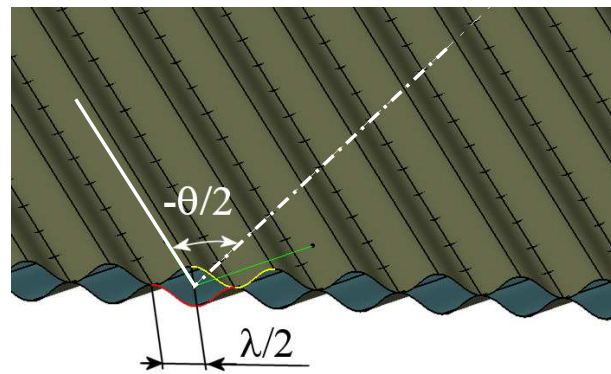
Figure 2.8 Costruction of the second corrugated surface on the top.

It is evident that the geometry has repetitive patterns in each direction so it is possible to cut the whole domain and consider the elementary periodic cell displayed

(a)

(b)

(c)

(d)
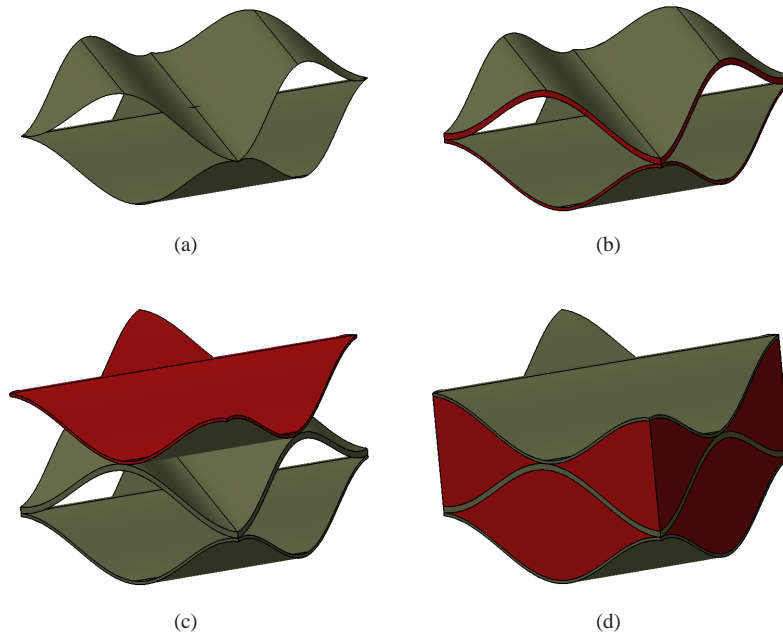
Figure 2.9 Different phases to generate the complete closed domain.

in Fig.2.9 (a) for the computation. As explained in detail in the next chapter, since the approach for heat transfer presented in this thesis requires the simulation of the flow and temperature fields in both cold and hot domains, the unitary cell is doubled, thus a thin solid layer has to be added to separate the fluid zones. The different phases of the construction of the final closed geometry are reported in Figs.2.9 (b), (c) and (d).

At least, another parameter defined as *Ltot* which is the global lenght of the heat exchanger has been prepared. Changing the parameter values, various different geometries can be automatically produced: for example, in Figs.2.10, 2.11 some new geometries have been obtained varying alternatively the cross-angle and the Bezier curves parameters.
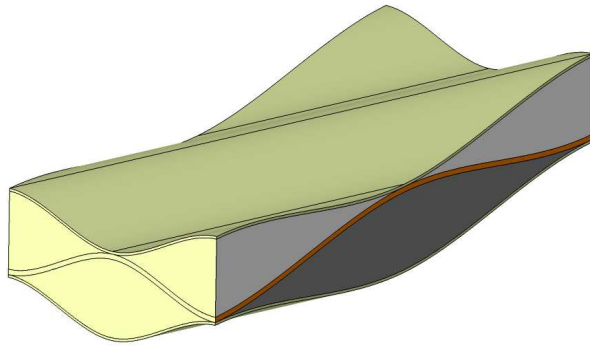
Figure 2.10 A possible geometry decreasing the cross-angle θ.
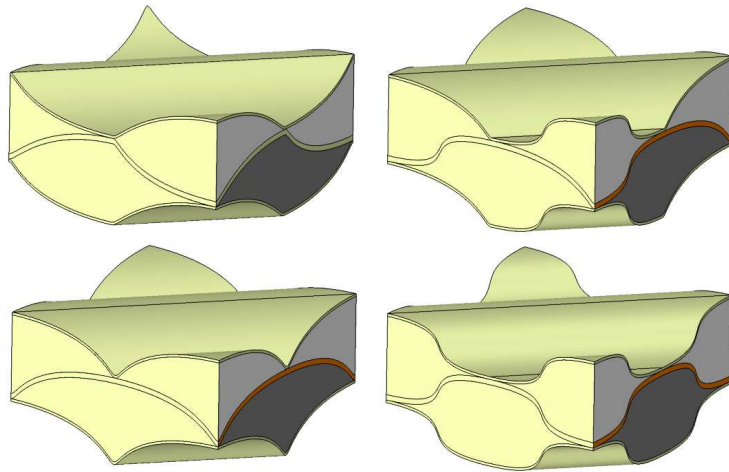
Figure 2.11 Some particular geometries obtained varying the Pi parameters.

Chapter 3

Numerical methodology

3.1 Introduction

The numerical simulation of the fluid flow and heat transfer capabilities of the cross-corrugated channels in a recuperator is a critical passage for a successful deployment of an automatic design methodology. In this framework the numerical simulation has to satisfy some important constraints, for instance the results have to be accurate but they must be obtained using reasonable computational resources too, so the simulation of the whole recuperator is clearly impracticable because it would require very high computational time.

To reduce the size of the computational domain, the symmetries and the repetitive pattern of the geometry can be exploited. Actually, after a short entrance region which can involve up to five modules, the flow and thermal fields become fully developed and repeat themselves from module to module in an identical or similar way [23]. Therefore it is possible to reduce the numerical analysis to the single periodic element using suitable periodic boundary conditions [16]. Such an approach is acceptable also in the present case of short heat exchanger if, as can be deduced from the data given in [15], the length of the device is equal to almost 15 or 20 modules.

As already reported in §1.4 various numerical approaches to the problem of heat transfer in periodic domains can be found in literature.

These previous studies on numerical simulation of cross-corrugated channels invariably restrict the analysis on a single module by imposing periodic conditions on velocity and pressure fields and solving the thermal field employing usually constant temperature boundary conditions [10, 11, 24]. Nevertheless for microturbine recuperators, constant flux boundary condition is deemed to suit better the real operative conditions, since the two flows are in counter current and characterised by similar heat flow capacities. In the following, the classical numerical treatments are presented along with a novel approach that couples cold and hot fluids in a periodic unitary cell.

To solve the fluid and thermal fields the commercial code *ANSYS CFX* has been

utilized. It uses a coupled solver, which solves the hydrodynamic equations for u, v, w, p as a single system. At any given time-step the solver uses a fully implicit dicretization of the equations. In case of steady state problems, as in this work, the time-step behaves like an "acceleration parameter", to guide the solution in physically based way to a steady-state solution, thus reducing the number of iteratons required to converge. *ANSYS CFX* uses a *Multigrid* (*MG*) accelerated factorization technique for solving the discrete system of linearized equations, approaching to the exact solution of the equations during the course of several iterations. For comparison purposes, the simulations have been also performed, in the validation phase of the methodology, with the commercial code *Fluent*.

3.2   Periodic boundary conditions

In the following the elementary periodic cell of Fig.2.9 (d) will be utilized. As already written, since the approach for heat transfer computation presented here requires the simulation of the flow and temperature fields in both cold and hot domains, the unitary cell is doubled. Moreover thin solid layers have been added since, when a conjugate heat transfer calculation is performed with the *CFX* code, the physical layers are required to separate fluid domains. The longitudinal heat conduction of the metal sheet can deteriorate the performance of the recuperator [25]. Nevertheless this effect has been discarded since the effectiveness reduction has been estimated to be below 1%.

From a fluid-dynamics point of view, the velocity field on both ducts is periodic in the mean flow direction, so pressure can be expressed as the sum of a linear term, depending on the pressure gradient α, and a periodic component $\tilde{p}$ as follows:

$$p(x, y, z) = -\alpha x + \tilde{p}(x, y, z) \tag{3.1}$$

Pressure and velocity on each point belonging to the periodic interfaces assume the same value, so it is possible to write:

$$\tilde{p}_i(y, z) = \tilde{p}_0(y, z)$$

$$\tilde{u}_i(y, z) = \tilde{u}_0(y, z)$$

$$\tilde{v}_i(y, z) = \tilde{v}_0(y, z) \tag{3.2}$$

$$\tilde{w}_i(y, z) = \tilde{w}_0(y, z)$$

while standard zero velocity condition has been assumed on solid walls. The pressure gradient term α can be added to the x moment equation as a source term.

Given that to each value of momentum source corresonds a value of mass flow, an iterative approach has been utilized to get the wanted value of mass flow, and so the Reynolds number, in case of a constant domain. In fact, thanks to the capabilities of the *CEL* language of *ANSYS CFX* code, a variable value of momentum source has been implemented as:

$$MomSource_i = MomSource_{i-1} + 0.3 * (MassFlow^* - MassFlow_{i-1}) \qquad (3.3)$$

where the new value of momentum source for the i iteration is given by the sum of its value in the $i - 1$ iteration added by a term proportional to the difference between the wanted mass flow $MassFlow^*$ and the calculated one. The convergence history of non-dimensional mass flow, during the iteration in a tipical calculation, is shown in Fig.3.1. It is possible to notice how the method converges monotonically in few iterations.

Besides, the temperature field is not periodic in a recuperator, since the temperature changes continuously along the cross-corrugated channel in the mean flow direction, so the analysis of the periodic fully developed temperature field needs a different approach and it follows a different pattern depending on the thermal boundary conditions.

Periodic heat analysis encountered in literature requires a single domain to be solved, as shown in Fig.2.9 (a), since suitable boundary condition must be applied on the walls, which means uniform temperature or wall heat flux prescribed on the primary surfaces.

Within the first method, a non dimensional periodic temperature can be defined if a uniform temperature is considered at the walls:

$$\tilde{T} = \frac{T - T_w}{T_b - T_w} \qquad (3.4)$$

where T_w is the wall temperature and T_b the bulk one defined as:

$$T_b = \frac{\int |\mathbf{W} \bullet \mathbf{n}| \, T dS}{\int |\mathbf{W} \bullet \mathbf{n}| \, dS} \qquad (3.5)$$

where S is the area of a surface normal to the mean flow direction and $\mathbf{W}$ is the velocity vector. For this case, the fluid temperature approaches more and more closely to the wall temperature, as the fluid flows through the channel, and the temperature

difference between fluid and wall decay exponentially to zero along the lenght of the duct.

If, on the contrary, the flux is prescribed on the boundary, temperature and pressure can be treated in a similar way, which means that temperature can be expressed as the sum of a periodic and a linear component driven by the gradient in the mean flow direction β:

$$T(x, y, z) = \beta x + \tilde{T}(x, y, z) \tag{3.6}$$

$$\tilde{T}_i(y, z) = \tilde{T}_0(y, z) \tag{3.7}$$

Eq.3.6 can be substituted into the energy equation:

$$\frac{\partial(\rho c_p T)}{\partial t} + \nabla(\rho c_p T \mathbf{W}) = \nabla(\lambda \nabla T) \tag{3.8}$$

to obtain the transport equation for the periodic component:

$$\frac{\partial(\rho c_p \tilde{T})}{\partial t} + \nabla(\rho c_p \tilde{T} \mathbf{W}) = \nabla(\lambda \nabla \tilde{T}) + \beta u \rho c_p \tag{3.9}$$

The last term in Eq.3.9 represents an energy source term that depends on the fluid velocity in the mean flow direction. Eq.3.9 can be solved with appropriate boundary conditions as in [24] where an uniform wall flux was imposed and, to satisfy the energy balance, the temperature gradient was computed as:

$$\beta = \frac{\phi}{\dot{m} c_p H} \tag{3.10}$$

where H is the length of the periodic module in the mean flow direction and ϕ the overall thermal flux specified at the walls. (It derives from $\phi = \dot{m} c_p \Delta T$ and $\beta = \Delta T / H$).

While the uniform flux is a practical solution for imposing a thermal boundary condition, it does not completely describe the heat transfer in a module of the recuperator, because the fluid flows in the furrows of the cross-corrugated ducts with complicated three-dimensional patterns, strongly affect the local heat transfer rates.

Since in this work the elementary periodic module is doubled to take into account both cold and hot fluids, Eq.3.9 can be applied to both domains and no boundary condition has to be imposed at the interface wall. To satisfy the global energy balance the same flux has been applied to the hot and cold domains by means of the *CEL* language also in this case:

$$\phi_h = -\phi_c \tag{3.11}$$

using Eq.3.10 to compute the source term of Eq.3.9. Temperatures of the hot and cold domains, are automatically adjusted and tend to fixed values during the iterative computation as shown in the non-dimensional chart in Fig.3.2, to satisfy the overall energy balance:

$$\phi = UA\Delta T \tag{3.12}$$

where ΔT is the bulk temperature difference between hot and cold fluids:

$$\Delta T = (T_{bi})_h - (T_{bo})_c = (T_{bo})_h - (T_{bi})_c \tag{3.13}$$

and U is the global heat transfer coefficient which depends on the heat flux distribution between the solid interface and the hot and cold fluids.
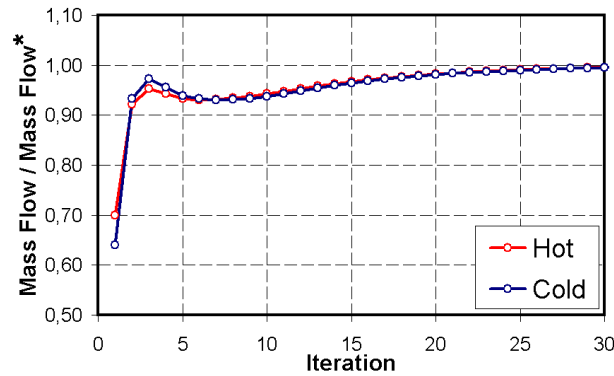
Figure 3.1   Convergence history of mass flow in hot and cold domains.

3.3   Mesh generation

The mesh generation process deals with the decomposition of a domain into finite elements in order to solve the partial differential equations. It is one of the most important and most time consuming step of a CFD analysis. The quality of the mesh plays a direct role on the goodness of the results, regardless of the fluid-dynamics solver used. Moreover the solver will be more robust and accurate when using a well constructed mesh. With these considerations, any CFD analysts have to know and judge all of the different kind of meshing criteria, i.e. structured or unstructured mesh, using as more as possible, different commercial/proprietary softwares, thus this phase
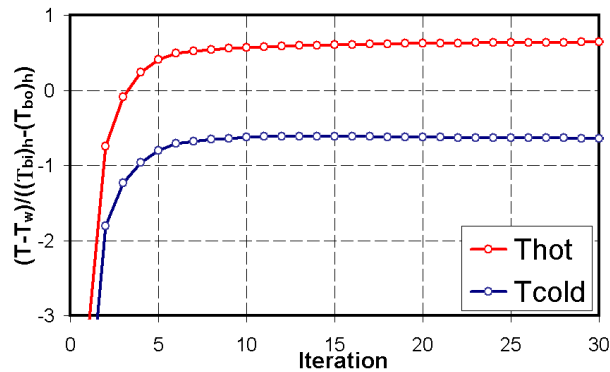
Figure 3.2   Convergence history of bulk temperature.

could be very time expensive.

In order to have a complete experience about this complicated choice, the package *ANSYS ICEM CFD* has been utilized, because it allows to generate meshes using various elements such as tetrahedrons, hexahedrons and prisms.

Below a brief description of the two main methodologies is presented with the basic advantages and faults.

Structured mesh method

Structured grids take their name from the fact that meshes have tidy structures arranged in regular repeating patterns called blocks. Generally, all interior nodes of the structured mesh have an equal number of adjacent elements. The approach is very effective when relatively simple geometry is considered but it could be used in mesh generation for complex geometries coupled with multi-block approach, in which the comlplete geometry is considered as whole of blocks. These blocks are further subdivided into elements, depending on the desired grid density. The block topology consists of information about vertices, edges, faces, blocks and their relationship among each other. Structured meshes offer more control over the size and shape of the elements. The main disadvantage of structured meshes is their lack of flexibility in covering the domains of complex shapes even if the grid can be shaped to the body fitted through stretching and twisting of the blocks infact they support a high amount of skewness and stretching before the solution will be significantly effected. The major

drawback of structured block grids is the time required to generate an optimal block structure for an entire model.

Below, the description of the step in order to generate a structured mesh with *ANSYS ICEM CFD* is given. After the model file has been imported, with both points, curves and surfaces as presented in Fig.3.3 (a), it is necessary to subdivide the main domain in smaller blocks as shown in Fig.3.3 (b), and assign the correlation between the edges of the blocks and the curves of the geometry by means the *Projection* function. At the end, it is necessary to define the number of nodes and eventually the thickening ratios on each edge of the domain.

(a) The model file, with points, curves and surfaces   (b) The blocks
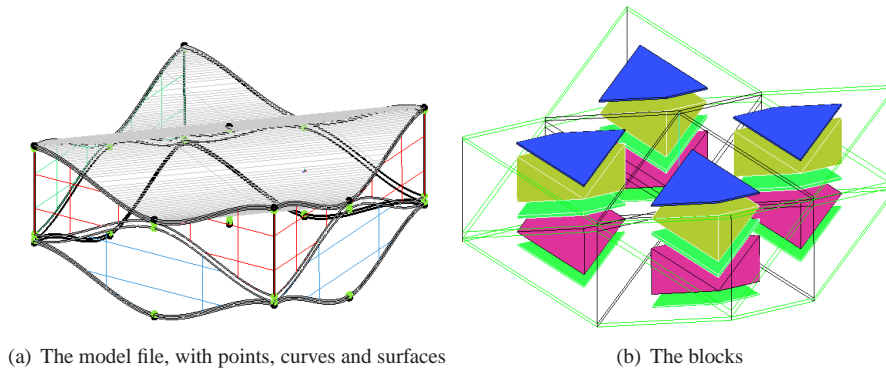
Figure 3.3   Two steps in order to generate a structured mesh with *ANSYS ICEM CFD*.

An example of the final mesh obtained by means of *ANSYS ICEM CFD* is illustrated in Fig.3.4.

Unstrucured mesh method

Tetrahedrons are the most widely used elements for 3D unstructured mesh generation since any arbitrary geometry can be more flexibly filled with this elements. Because the arrangement of elements does not have recognizable patterns, the mesh is called unstructured. The main disadvantage of unstructured meshes is that the control over the size and shape of elements is very difficult so usually a large number of elements is needed to discretize even not complicated geometries and this unfortunately leads to high computational time. On the contrary, the main advantage of the unstructured generation method is the large degree of automation of this method, therefore, it requires less time and efforts.
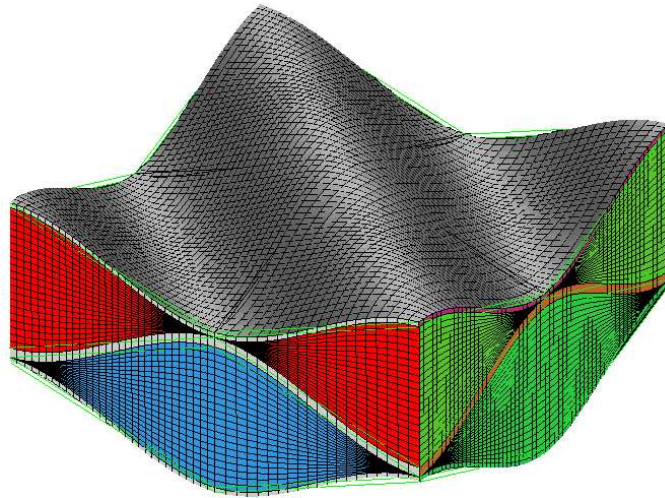
Figure 3.4 Structured Mesh.

Starting from a clean CAD model (surfaces, curves and points) and a global reference size of the elements, a good mesher can automatically generate triangles on the surfaces and tetrahedra in the volume by successive refinement until all grid density requirements are met. Moreover, maximum element sizes can be defined on different surfaces or volumes to refine areas where a high gradient in the flow field is expected. The resulting tetrahedral mesh is an adaptive mesh of non-uniform density and it is independent of the CAD patch structure.

Hybrid mesh method

Hybrid mesh methods are adopted to take advantage of the positive aspects of both structured and unstructured grids utilizing structured grid in restricted regions and unstructured grid in the bulk of the domain. The various elements, such as hexahedral, tetrahedral, prismatic and pyramid elements in 3D are used according to their strenghts and weaknesses. The ability to control the shape and distribution of the grid locally is a tool that can lead to excellent meshes.

ANSYS ICEM CFD can arrange layers of prism elements near the boundary surfaces, controlled by exponential or geometric growth laws, in order to appropriately model close to wall physics. As a result, it generates a hybrid tetrahedral grid con-

sisting of prism elements near the walls and tetrahedral elements in the interior of the space to be meshed. The hybrid mesh of the single domain obtained with *ANSYS ICEM CFD* and a detail of the prism layers are shown in Figs.3.5, 3.6.
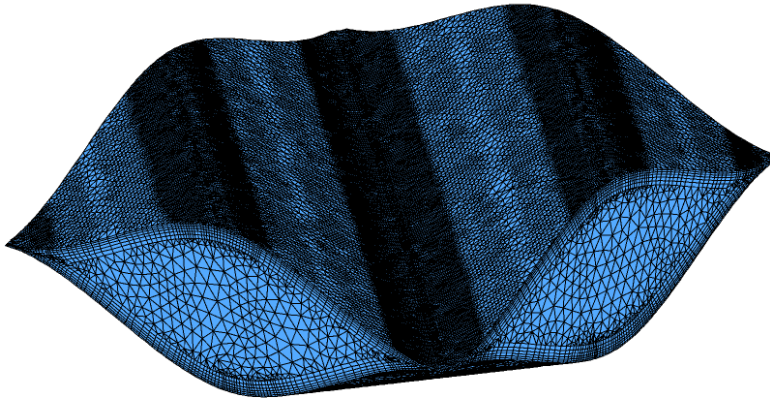
Figure 3.5 Hybrid mesh.

3.4 Validation of the results

To validate the methodology, the results of the present simulations need to be compared with the literature data. As observed while discussing the numerical methodology, it has been impossible to find in the open literature experimental data for the considered surface geometry and Reynolds number range, so that the comparison was carried out only on the basis of numerical data. Moreover, to be sure that the CFD predictions did not feel the effects of the grid and to compare the results between the two different mesh approaches, several grids have been simulated at various Reynolds number, increasing gradually the number of elements to obtain a mesh independence analysis.

For first the hybrid method has been validated, testing eight different meshes from coarse with both few and many prisms layers to extremely fine, obtained changing the parameters in *ANSYS ICEM CFD*, like the global dimension of the elements (which is
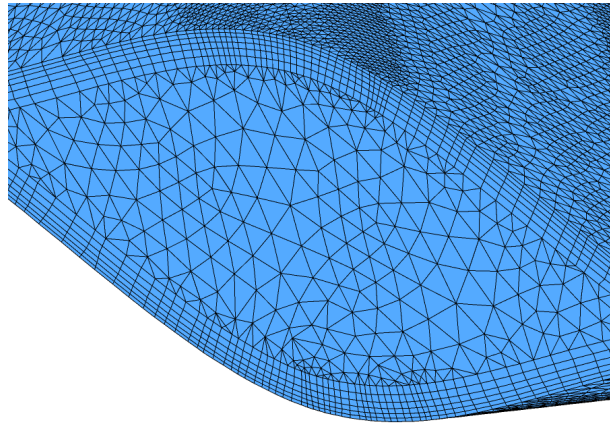
Figure 3.6 Detail of the hybrid mesh.

related to the total number of cells) and the number or the thickness of prisms layers.
The details of meshes are listed in Tab.3.1.
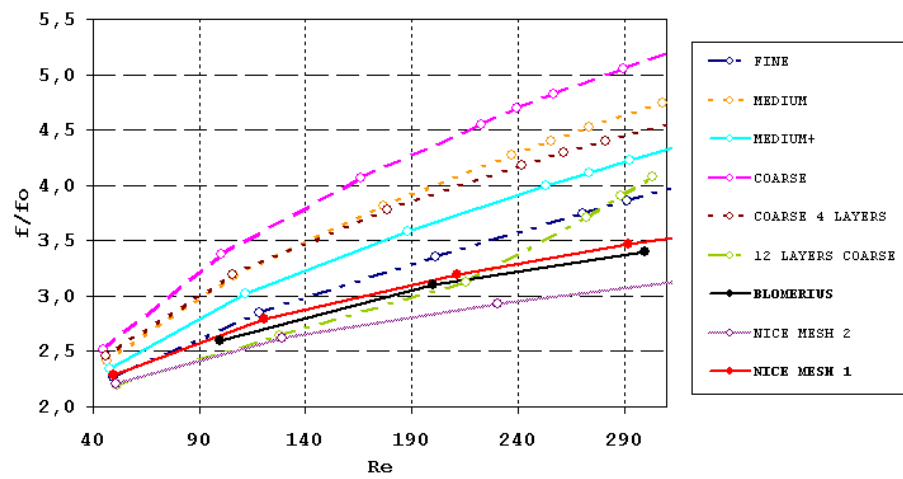
Figure 3.7 Grid Independence.

name	elem	layers
FINE	864886	1
MEDIUM	206440	1
MEDIUM+	449584	2
COARSE	111733	1
COARSE 4	134700	4
COARSE 12	185138	12
NICE MESH 2	626124	6
NICE MESH 1	704591	6

Table 3.1 Mesh independence for unstructured grids.

	Nodes X,Y	Nodes Z	CELLS	Time min.
A	26	16	82500	29
B	31	21	154800	49
C	36	26	259700	80
D	41	31	403200	117
E	46	36	591300	157

Table 3.2 Mesh independence for structured grids.

The values of the non-dimensional friction factor, which is $f = \alpha 2b/(2\rho u^2)$ divided by $f_0 = 24/Re$ relative to a fully developed laminar flow between two straight plates, obtained at different Reynolds number, compare very favourably with those of literature [18] as shown in Fig.3.7. However, given that a very fine mesh is needed to cover the literature data, a huge computational time should be required in the optimization phase where hundreds of simulations are required. Thus, to reduce the amount of cells and so the calculation time and resources, the structured approach is needed.

To obtain the structured mesh-invariance, five meshes have been calculated. The details of the number of nodes on X, Y and Z directions and complessive number of cells are indicated in Tab.3.2.

The structured grid presented in Fig.3.4 is composed by 154800 hexaedra cells (Case B), and has been selected as a trade-off between accuracy and computational costs. Computations with refined grids up to 591300 (Case E) hexaedra elements have been carried out to obtain the mesh independence as reported in Fig.3.8.

On the left side of the figure there is a percentage scale for the thermo/fluid dynamics behaviors, instead on the right there is a time scale in minutes. It is possible to notice that thecomputational time raises almost linearly, as the thermal-hydraulic values tends to 100%. It has been verified that the coarser mesh used in this work involves a maximum error estimated of 0.5% for the ΔT number and 0.3% for the momentum source, moreover it can be noticed that to reduce the error less than 0.2%, a mesh with more than 250000 elemets is needed (Case C), but this choice should cause an increase of CPU time consuming from 50′ up to 80′, as reported in table 3.2.
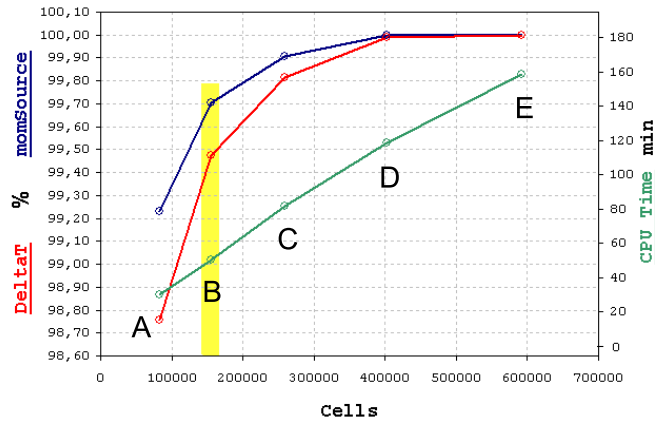
Figure 3.8 Grid independence.

Figure 3.9 reports the normalised friction factor f/f_0 for the selected Case B, where $f_0 = 24/Re$ is relative to a fully developed laminar flow between two straight plates, as a function of the Reynolds number.

In the same manner, the Nusselt number, normalized with straight plain channel value $Nu_0 = 7.537$, is plotted in Fig.3.10 at different Reynolds numbers. The results obtained with the proposed method with the *ANSYS CFX* code give higher heat transfer rates than those reported in literature and those obtained with the *Fluent* code, all characterised by prescribed uniform temperature boundary conditions.

The complicated nature of the flow and thermal fields in the cross-corrugated channel can be visualised by means of the temperature contours and velocity vectors plotted in the reference planes of Fig.3.11.

The periodic temperature and velocity fields in hot and cold domains are respectively presented in Fig.3.12 and Fig.3.13. The distribution indicates a strong depen-
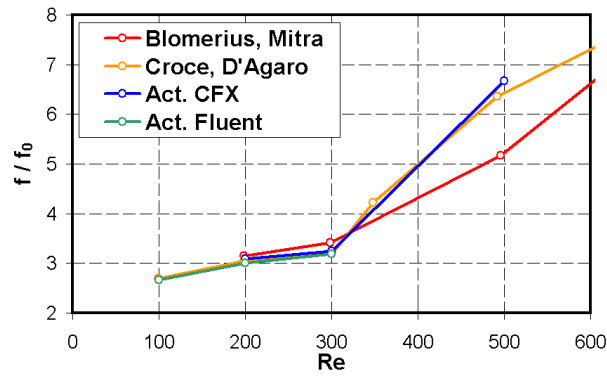
Figure 3.9 f/f_0 comparison.
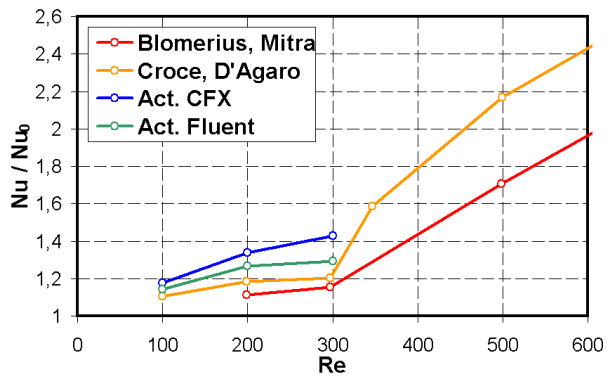
Figure 3.10 Nu/Nu_0 comparison.

dence on the complicated flow field that is forced to follow the furrows of the channel changing direction and impinging on the walls.

In Fig.3.16 the distribution of local Nusselt number on the top and bottom walls is shown. It can be clearly seen that the pattern is well away from an uniform distribution, because, as stated before, the heat flux depends heavily on the complicated nature of the flow field in both domains. Higher values of local heat transfer are attained at the points where the flow first impinges on the wall and then deviates to follow the

channel geometry.
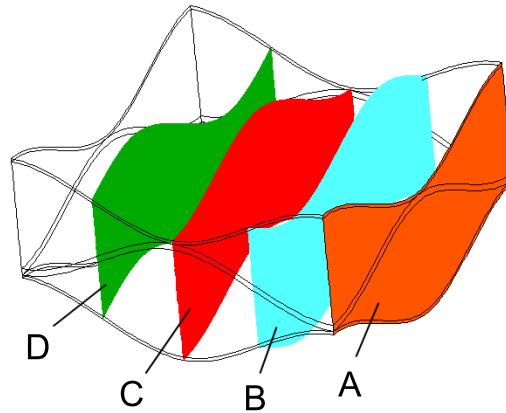
Figure 3.11   Cross sections for plot visualization.

The analysis of the velocity vectors of Fig.3.14 reveals a steady regular flow and two distinct streams which follow the furrows between the corrugations of the plates. The pattern of the flow between the corrugated plates is also plotted with streamlines in Fig.3.15, in which two streams that tend to mix are clearly visible. This mixing effect gives a contribution to the enhanced heat transfer characteristic of the cross corrugated channel.
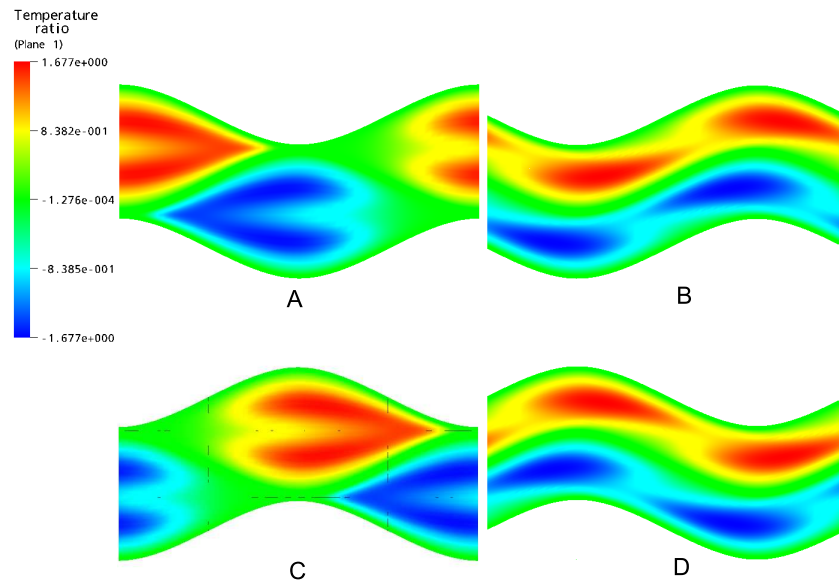
Figure 3.12   Temperature contours on each section.
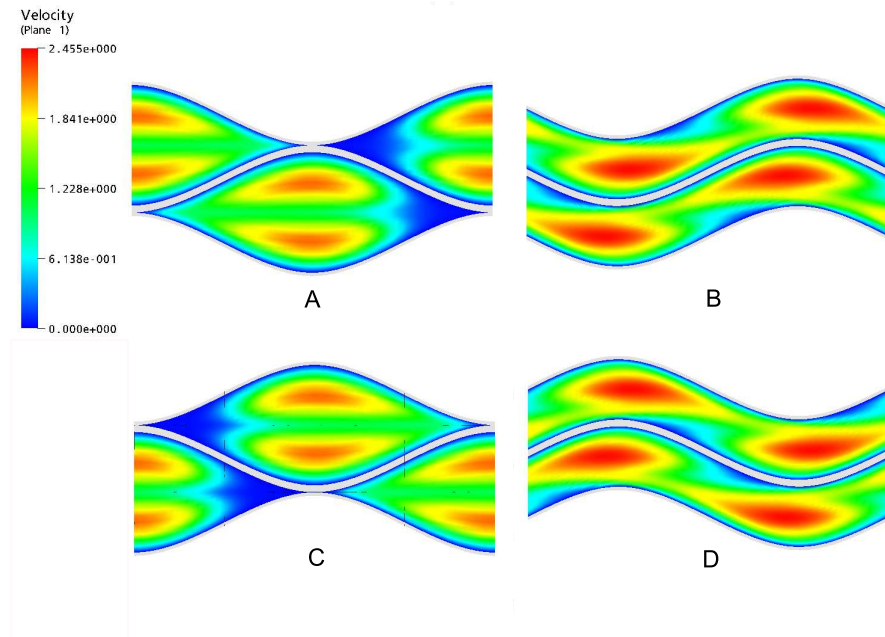
Figure 3.13   Velocity contours on each section.
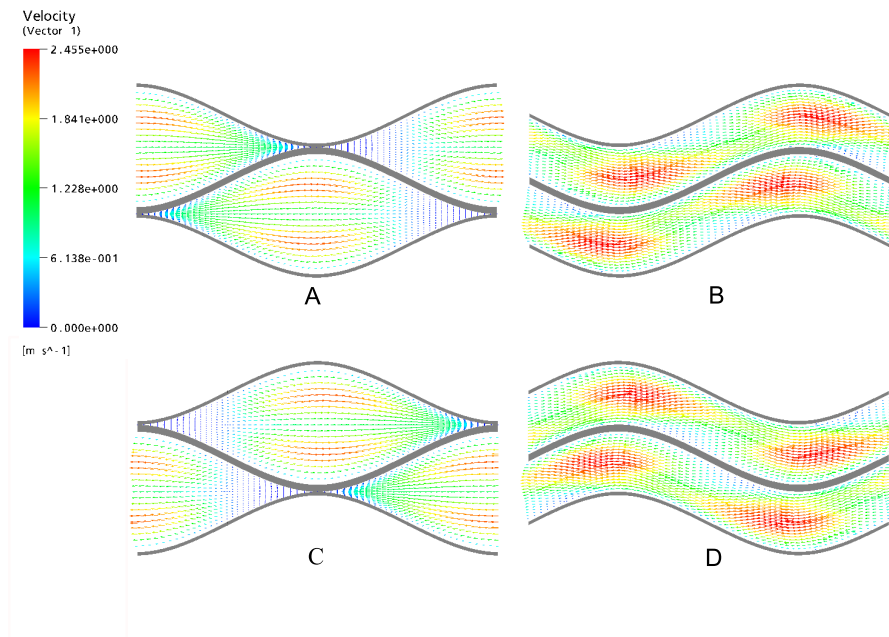
Figure 3.14 Vectors on each section.

Figure 3.15 Streamlines.
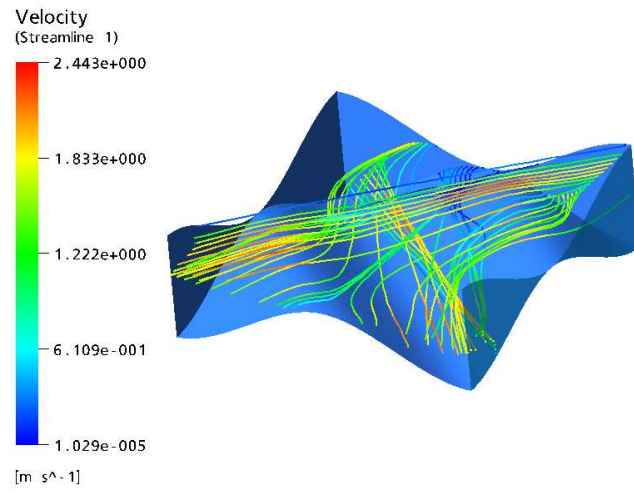
(a) Top surface   (b) Bottom surface
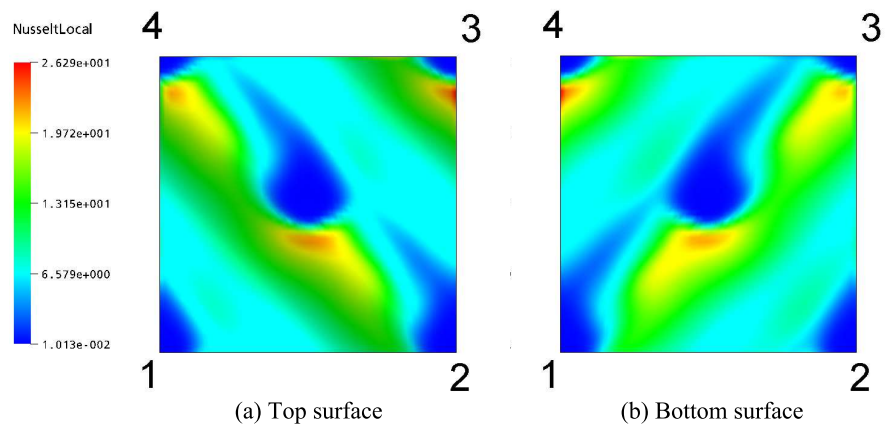
Figure 3.16 Nusselt number on the top and bottom surfaces.
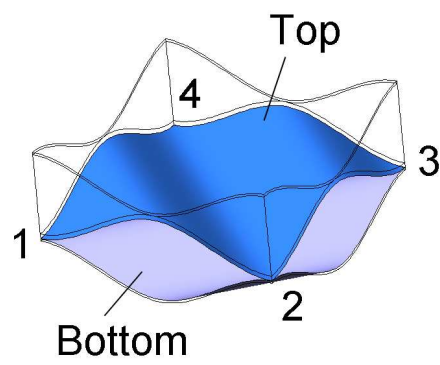
Figure 3.17 Wall surfaces for plot visualization.

Chapter 4

Multi-objective optimization

4.1 Introduction

In the previous chapter the results of the simulations of the cross-corrugated recuperator, with a 90° cross angle, have been successfully validated by comparison with literature data, thus it can be assumed that also the other different geometrical shapes, which will be generated during the automatic optimization procedure, could be reliably analyzed and compared.

When a complex engineering design is performed, it is not possible to carry out a single optimization phase, because often it is hard to define *a priori* all the parameters involved into the optimization. Usually, during the development of the project, it is necessary to change the ranges of some constraints, to fix or add some design variables, or, in multi objective case, to change the number of the optimization criterions.

Therefore, there is the necessity to use a process integration environment to help the designers in the optimization phases by means of statistical tools. As explained in [26], the statistical analysis for reducing the number of design variables is an important tool for limitating the total number of simulations needed to get the best final design. For these reasons the optimization platform *modeFRONTIER* [27] has been utilized, because it is a complete software and it implements several features as:

- *modeFRONTIER* is the only truly multi-objective commercial product on the market, as it is able to manage many goals at the same time, allowing to pick the best design at the end of the optimization, from a set of designs that represent the best designs for various trade-offs;

- the various exploration and optimization algorithms can be mixed at will, so that powerful hybrid optimization techniques can be easily implemented.

- it uses a small number of highly efficient and proprietary algorithms;

- it embeds non-linear response surfaces, which can be used to speed up the optimization of complex problems;

- it is possible to change goals and constraints during the optimization phase which allows to steer the optimizer towards regions of the design space that are more appealing, but not predicted before starting the optimization;

- it is intuitive to use thanks to its *GUI* (Graphical User Interface) by means of which it is easy to describe the problem, define a set of constraints on the input and output variables, and express the goals.

In this chapter, two series of optimization of microgas turbine recuperator, using the Multi Objective Genetic Algorithm (*MOGA*) strategy, are presented: the first has been useful to better understand the problem (which variables are the most influent, which objectives are really interesting) and the second one has the aim to find out the final optimal design. The description of the main concepts, as *design variables*, *objectives* and *optimization strategies*, are given in order to better understand the different phases when formulating an optimization problem.

4.2 Design variables

Design variables are parameters that can be adjusted in order to modify the system to design. There are many types of variables [28]:

- *independent design variables* are the quantities the designer deals with directly, such as geometry, material properties, configuration of components and many more. Independent design variables are usually called just design variables or design parameters.

- *dependent variables* are variables the designer can not directly assign values to, but working with them through the design parameters. The dependent variables are usually named *characteristics* or *attributes* of the design. Examples of system characteristics are energy consumption, pressure drop and cost. The quality of a design is largely a function of its characteristics. In optimization, the objective function value corresponds to the value of a particular characteristic. An objective function is thus the relation between the design parameters and this characteristic. For a general design problem, it might be very difficult or even impossible to represent all such relations analytically because, as in this thesis, the characteristics are the outcome of complex simulations.

- *state variables* are an intermediate type of design variables between dependent and independent design variables, such as the pressure in a hydraulic cylinder or the current to an electric motor. State variables cannot directly be assigned values, and they do not directly contribute to the value of the design, as the characteristics do.

- *operating variables* are variables that can be changed by the operator after the design has been actually built.

- *environmental variables* or the *external variables* are the environmental factors that affect the design when in use, e.g. changing mass flows or temperatures.

The design problem could be formulated as to assign values to the system parameters to ensure that the state variables and the characteristics are as good as possible during a wide range of operating and environmental variables.

Regarding the heat exchangers, the independent geometric variables could be, as an example, the tube diameter and length or the number of tubes in case of conventional shell-and-tube recuperators (see §1.3.1), or the geometry fins geometry, angle and size in case of tube-fin type (§1.3.2). On the contrary, the geometric variables for a cross-corrugated recuperator basically are, as already clarified in §2.4, the parameters that modify the shape of the primary surface involved in the heat exchange, the corrugation angle given by the crossing plates, the hydraulic diameter of the flow passages and the total length of the exchanger. Besides, given that in heat exchangers, thermal phenomena are involved, it is possible to consider the temperature difference of the fluids and the mass flow rate (or velocity) as the operating variables. Dependent variables instead, could be the heat transfer rate and the pumping power (or pressure drop).

All these variables may have intrinsic complicated relationships and obviously have influence on the performances of the recuperator, so often the way to classify a characteristic as a good or bad one, which means to choose or formulate an objective, could be very awkward. Therefore the presence of system and design constraints leads to a large number of methods to classify the goodness of a design, also known as *Performance Evaluation Criteria* (*P.E.C.*). The details and the main classification of these strategies are given in the next section.

4.3 Performance Evaluation Criteria

A Performance Evaluation Criteria is established by selecting one of the operational variables as a performance objective, in accordance with the constraints on the remain-

Case	Geom.	massFlow W	Pump.Power P	Heat flux q	ΔT	Obj.
FG-1a	N,L	X	-	-	X	$\uparrow q$
FG-1b	N,L	X	-	X	-	$\downarrow \Delta T$
FG-2a	N,L	-	X	-	X	$\uparrow q$
FG-2b	N,L	-	X	X	-	$\downarrow \Delta T$
FG-3	N,L	-	-	X	X	$\downarrow P$
FN-1	N	-	X	X	X	$\downarrow L$
FN-2	N	X	-	X	X	$\downarrow L$
FN-3	N	X	-	X	X	$\downarrow P$
VG-1	-	X	X	X	X	$\downarrow N*L$
VG-2a	N*L	X	X	X	X	$\uparrow q$
VG-2b	N*L	X	X	X	-	$\downarrow \Delta T$
VG-b	N*L	X	-	X	X	$\downarrow P$

Table 4.1 Performance Evaluation Criteria for smooth circular tubes.

ing variables of the design. Common thermal-hydraulic goals include reducing the size of the recuperator required for a specific heat rate, increasing the heat transfer of an existing recuperator manteining constant the pressure loss, reducing the approach temperature difference or reducing the pumping power for equal heat rate and length of the exchanger.

Several authors [29, 30, 31] have proposed the classification of the performance evaluation criteria in three main categories: *FG criteria*, by means of which the cross-sectional envelope area and lenght are held constant, *FN criteria* that maintain fixed the flow frontal area, but allow the lenght of the heat exchanger to be a variable and the *VG criteria* which is used when the *FG* and *FN* criteria are not applicabile because the recuperator is sized for a required thermal duty with specified flow rate. These groups of constraints are applicated in case of smooth circular tubes, as indicated in Tab.4.1, choosing two of the following objectives: reduction of the approach temperature difference, reduction of the pumping power or reduction of the length of the heat exchanger L, where N is the number of tubes. However, even though these criteria seem to be complete, they take it for granted some thermal-hydraulic comparisons that instead could be applied only to basic geometries, like smooth circular tubes of shell-and-tubes evaporators. Thus a full analysis of the enhancement effect may require consideration of the entire system, much more in cases when the flow rates or temperature levels change as a consequence of the enhancement itself.

4.4   Formulating the objectives

As most optimization problems are multiobjective in nature, there are many methods available to tackle this kind of problems. Generally, the multiobjective optimization problem can be handled in four different ways depending on when the choice concerning the different objectives is made: never, before, during or after the optimization procedure. In the first two approaches, the different objectives are aggregated to one overall objective function. Optimization is then conducted with one optimal design as the result. Thus it is strongly dependent on how the objectives were aggregated. The easiest and perhaps most widely used method to aggregate the objectives is the weighted-sum approach. The objective function is formulated as equation (4.1):

$$min \sum_{j=1}^{k} \lambda_j f_j(\mathbf{x}) \ : \quad \mathbf{x} \in S, \ \ \lambda \in R^k | \lambda_i > 0, \ \ \sum \lambda_i = 1 \qquad (4.1)$$

where λ_i is the weight relative to the i objective. As the objective functions are generally of different magnitudes, they might have to be normalized first. Although the formulation is simple, there is no clear relation between the weights and the obtained solution.

The third approach is an iterative process where the preferences on the different objectives are progressively changed. The basic assumption of this method is that it is easier to estimate the objectives once the search for an optimal solution has yet started.

In the fourth and last approach, optimization is conducted without the interference of the designer among the objectives. The outcome of this optimization is a set of optimal solutions which elucidate the trade-off between the objectives, which is called *Pareto* set. The decision-maker then has to compare the better desings in order to select which is the best one. The big advantages with these types of methods are that the solutions are independent from a subjective human preference. The analysis has only to be performed once, as the Pareto set would not change as long as the problem description remains unchanged. However, some of these methods require large computational time and resources. Another disadvantage might be that at the end of the optimization there are too many solutions to choose from. One of the techniques that allow to search in the solution space a set of Pareto optimal solutions and then present them to the designer is the *Genetic Algorithm*, which will be treated in the next section.

4.5   Optimization strategies, Genetic Algorithm

Optimization methods could be divided into derivative and non-derivative methods. This thesis focuses on non-derivative methods, as they are better suited for general design problems. Non-gradient methods are more robust in locating the global optima and are applicable in a broader set of problem areas. Another advantage of non-derivative methods is that they do not require any derivatives of the objective function in order to find the optimum. Hence, they are also known as black-box methods. In this thesis the objectives are results of computer simulations, thus the derivatives of the objective function are not explicitly known. The disadvantages are however that it is impossible to prove that the actual optima have been found. Nevertheless, by conducting several optimizations with different initial conditions, it could be made probable that the global optimum is truly found. Another disadvantage with non-gradient methods is that they usually require more function calls than gradient methods, and are thus more computational expensive. However, as the capacities of the computers are increasing this disadvantage is diminishing. Furthermore, most non-gradient methods are well suited for implementation on parallel processors. There is a large number of non-derivative methods, for example, the Simplex method and its constrained version named Complex developed in the 60's, the Genetic Algorithm or the similar Evolutionary Algorithm, both developed in the early 70's or the Simulated Annealing developed in the early 80's. Apart from these methods, there are also other promising techniques to conduct engineering optimization, for instance response surface approximations (*RSM*), as well as Taguchi methods.

The method adopted in this thesis which is the Genetic Algorithm (*GA*), carries out the optimization as the problem solution of competition among a population of evolving candidates. So, the basic idea is that the genetic pool of a given population potentially contains the better solution to a given adaptive problem.

Every individual is characterized by a binary string (the *chromosomes*) composed by *genes* which encode the activation or deactivation of a feature, and a fitness value which is assigned to it. The fitness function determines how well a design is able to solve the problem which is represented by the objectives of the optimization.

During the reproductive phase, individuals are selected from the population and recombined, producing offspring that will be the next generation. The recombination of the chromosomes of the parents could be realized in different ways. The most used operations to modify the genes of the individuals, to obtain the new generation, are:

- the classical *cross-over* operator which is the coupling of two individuals to create two new designs cutting the chromosome strings of the starting generation at some randomly chosen position. This fact produces two "head" segments, and

two "tail" segments. The tail segments are then interchanged to generate two new full length chromosomes as shown in Fig 4.1. The cross-over probability P_{cr-ov} can assume values between 0.0 and 1.0, where a null value means that cross-over is not applied and new generation is produced simply by duplicating the parents, so usually a value near 0.5 is chosen.
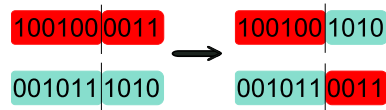
Figure 4.1 Classic crossover.

Moreover, *modeFRONTIER* implements an improved method called *directional cross-over*, that creates new designs considering the fact that a direction of progress can be evaluated by comparing the fitness values of individual Ind_i from generation t with the fitness of its parents Ind_j and Ind_k belonging to generation $t-1$. The new individual is then created by moving in a randomly weighted direction that lies within the ones individuated by the given individual and his parents as shown in Fig.4.2.
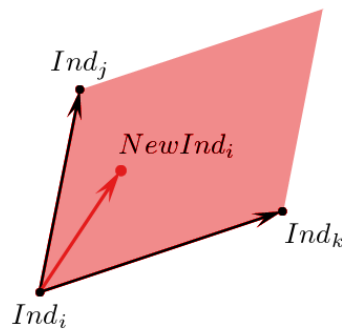
Figure 4.2 Directional crossover between individuals Ind_i, Ind_j and Ind_k.

- the *selection* operator chooses designs with the best fitness, or value of the function, and replicates them into the next generation, which means that a good solution has more probability to survive than a bad one. As for the cross-over operator, it is characterized by a P_{sel} probability value between 0.0 and 1.0

which gives the probability that design configurations are not changed during the evolution.

- the *mutation* is the operation by means of which some bits (*genes*) of some individuals are randomly changed in order to avoid a premature convergence increasing the possibility of covering all the designs space. This operator is distinguished by two parameters: *probability of mutation* and *DNA String Mutation Ratio*; the first, P_{mut} gives the probability that a design configuration is randomly perturbed. If the value is 1.0, the algorithm becomes a pure random search. The mutation probability should be kept at low values, usually smaller than 0.2. A mutation rate equal to 0.1 is the default value as in small population cases (typical of design optimization application) variability in the search process is recommended. If the sum of probability of directional cross-over, probability of selection and probability of mutation exceeds the value of 1.0, the following rule is applied:

$$P_{mut} = 1 - (P_{cr-ov} + P_{sel}) \qquad (4.2)$$

The second parameter, *DNA String Mutation Ratio*, value gives the percentage of the individual chromosome that is perturbed by the mutation operator so it defines the number of bits that mutate. If the mutation ratio is 0.0 none of the bit are modified. A value of 1.0 will change all the bits.

4.6 Optimization applications

In order to preparate and run an optimization process with *modeFRONTIER* environment, there is the necessity to define all the settings required by the software, by means of the *grafical user interface*, as shown in Fig.4.3. In this diagram, a typical process flow is represented, in which the imaginary flow chart of the optimization process goes from the left to the right, where respectively the design variables and the objectives are arranged. In the middle of the flow instead, there is a chain of icons whose task is to run in batch - by means of shell scripts - the executables of the software utilized to run the simulation which goes from the *CAD* tool, mesh generator and CFD pre-processor, to the fluid-dynamics solver and post-processor. As already said in the introduction, two serial optimizations have been performed and reported in this chapter because of the importance at the beginning, to investigate the ranges of variation of the variables, with the aim to not limitate the possible solutions. In a second *a posteriori* optimization, the ranges can been adjusted in order to focus the results and find better design solutions, as discussed in §4.6.1 and §4.6.2.
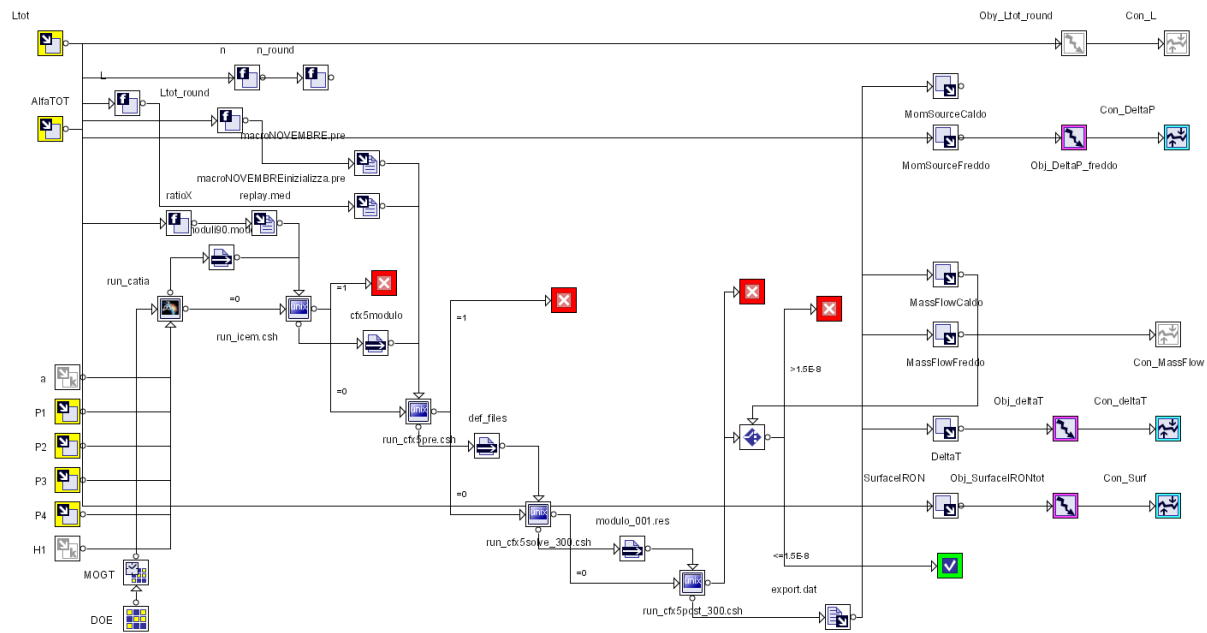
Figure 4.3   Process Flow of *modeFRONTIER*.

Variable Name	Min Value	Max Value	design_0
$P1$	0.8	1.2	1.0
$P2$	0.8	1.2	1.0
$P3$	0.8	1.2	1.0
$P4$	0.8	1.2	1.0
$Ltot$	$110mm$	$130mm$	$118mm$
θ	$58°$	$62°$	$60°$

Table 4.2 Initial variables range, first optimization.

4.6.1   Primary Optimization

In the first optimization, six geometric variables defined in 2 ($P1$, $P2$, $P3$, $P4$, $Ltot$, θ) have been chosen, because they have been catalogued as the most influential parameters as regards thermal and hydraulic behaviors (§2.4). Three main ojectives selected in agreement with the performance evaluation criteria are: to minimize the pressure drop between inlet and outlet and this is correlated to the required pumping power, to minimize the bulk temperature difference between the two fluids, which is connected to the global heat transfer coefficient and to minimize the total surface of the recuperator which is proportional to the final cost of the material needed to manfacture the recuperator.

To ensure that the final optimum design would have good performances in comparison with a reference one which is nicknamed *design_0*, each objective has been coupled with a constraint: the values of the constraints have been selected considering the calculated performances of the geometry characterized by a corrugation angle $\theta =$ 60°, indicated by Stasiek et al. [14] as a good compromise in terms of heat transfer rate and friction factor. Moreover the ranges of the variables listed in Tab.4.2 have been reasonable chosen around the values of this reference geometry.

To start the optimization, it is necessary to initialize the algorithm, selecting the first set of design to be evaluated. There are many different methods to select as more as possible representative groups of individuals; these methods are usually catalogued as "Design of Experiment" (*DOE*). This term was originated around 1920 by the British scientist R.A. Fisher, who studied this systematic approach to sample the design space, and to maximize the knoledge gained from experimental data, providing information on the major interactions between the variables. Prior this method, the traditional approach was to test one variable at a time, which meant that this factor was varied helding costant the other factors. By using this old technique, many eval-

uations were ususlly needed to obtain the sufficient information. The *DOE* approach overcame the traditional method as it consider all the variables simultaneously, changing more than one variable at a time thus eliminating redundant observations, reducing the time and resources to make esperiments which means to achieve the most relevant information with the minimal effort.

When using an optimization tool such *modeFRONTIER*, apply *DOE* is very useful because it allows to get a good understanding of the problem by identifying the sources of variation and to find a good starting point for an optimization algorithm.

In general, a good distribution of points obtained by means of a *DOE* technique, will extract as much information as possible, examining as few data as possible. There are several *DOE* provided by *modeFRONTIER*, so for each kind of problem to face, the designer has to choose between different methods listed below:

- *Exploration DOEs*, useful for getting information about the problem. This methods, that allow good sampling of a configuration space, can serve as the starting point for subsequent optimization processes. They are subdivided in: Random, Sobol and Monte Carlo.

- *Factorial DOEs*, a large group of techniques essential to perform statistical analyses to highlight possibles interactions between variables. Some of the whole are: Full and Reduced Factorial, Cubic Face Centered and Latin Square. Reduced factorial attempts to provide a reasonable coverage of the experimetal space while requiring fewer experiments.

- *Orthogonal DOEs*, useful to identify the main effects and all the interactions between variables. They are: Taguchi Matrix and Plackett Burman.

The choice of *DOE* depends on the type of objectives and on the number of variables involved. Whenever *DOE* is used during the optimization process, it should always be applied before the actual optimization phase as it can be useful to reduce the number of variables and to limitate the range of variations.

For the first optimization, an initial *DOE* constituted of 39 designs obtained by *Sobol* method in addition with the original *design_0* has been chosen. This is a usual procedure to increase the speed of convergence when a reference design is available. The number of designs needed as the first population can be usually calculated by a simple correlation which says that to describe in good manner the variables space, the number of designs of the initial generation has to be greater than the product of the double number of variables multiplied by the number of objectives.

The multi-objective optimization managed by the genetic algorithm $MOGA - II$ available in *modeFRONTIER*, has been stopped after 15 generations, and 600 overall calculated designs.

From the observation of the convergence profiles of the three objectives in Fig.4.4, it is possible to notice how the optimization algorithm works in two different phases; in the first (from the design id 1 to around 250), the algorithm finds the feasible geometries that satisfy the imposed constraints; this phase is characterized by an high instability, index that the algorithm explores different regions in the variables space. In the second phase (from design 250 to the end), the algorithm finds the variables region with the best compromise between the objectives, so it becomes to convergence.

An interesting and useful aspect is to analyze the influence of the design variables in the design performances. Two are the important points of this work phase: to understand which are the most important variables or if there are some unuseful, and to understand if the variable ranges are properly fixed.

To explain these two points, both the convergence profile of the variables and the *t-student* parameter have been used thanks to the tools of *modeFRONTIER*. The *t-student* parameter is a statistical tool to explain if two data distributions are really different, and it could be used to understand the influence of the variables.

From the observation of the Fig.4.5, it is possible to argue some interesting remarks: first it is easy to observe that the ranges of the variables have not been set with correct values, because during the optimization, the algorithm has found many designs with the lower range value. This fact could lead to a probability that, relaxing the variables ranges, it would be possible to find better solutions in terms of objective function values. This behavior happens explicitly for the variables: $P2$, $P3$, $P4$ and θ.

The relationships between the objective functions and the variable L_{tot} is quite different, in fact, from the variable convergence profile, it is possible to notice how the algorithm fixes the value of this parameter to 118 *mm* after 240 designs (6 generations), to not exceed the constraints. This trend happens because the total length of the recuperator has revealed to be the most influential geometric variable in this design phase, thus almost infinitesimal changes in this parameter lead to great variations of the thermal-hyraulic performances up to violate the constraints; this fact is more evident from the *t-student* charts of the objectives with regard to the geometreic variables in Fig.4.6. In these charts the blue bar corresponds to the *Significance* of the variable which indicates whether there is a relationship between it and the objective functions. The orange bar instead represents the *Delta* parameter, that shows how strong a relationship is. A *Delta* parameter greater than zero shows a direct correlation with the design variable, a negative value indicates that the relationship is inverse, so it creates

(a) DeltaP

(b) DeltaT

(c) Surface
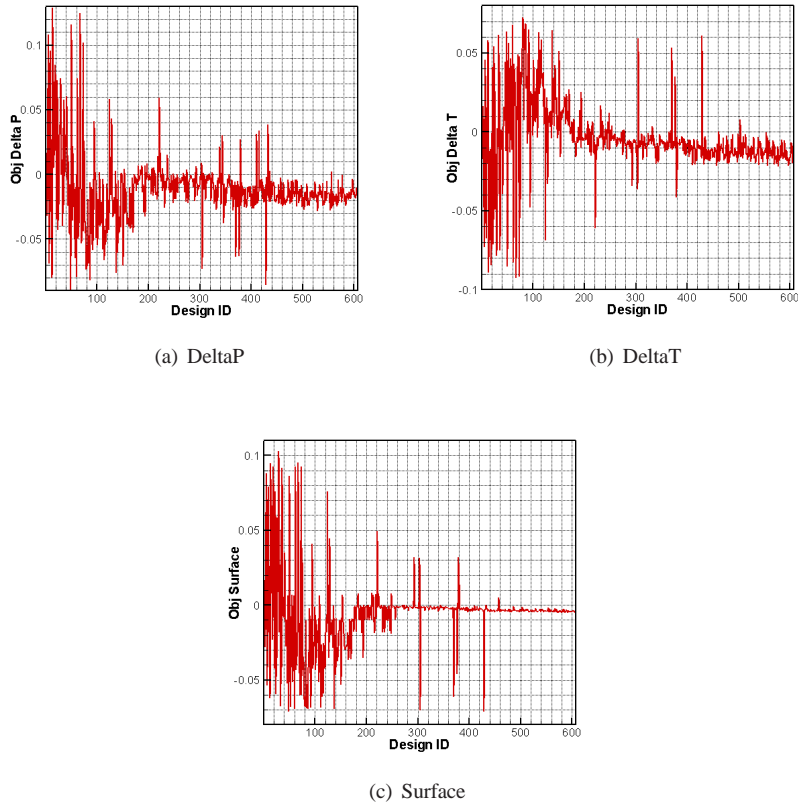
Figure 4.4 Objectives History Charts, I optimization.

a sort of ranked list of importance. Low value parameters indicate that there are no correlations between variable and performance, so it would probably be possible to ignore these variables in the following analysis. From Figs.4.6 (a) and (b) is it possible to notice that the whole parameters have highest significances but only the L_{tot} parameter has high absolute value of *Delta*. In detail, L_{tot} has *Delta* = −100% for the *DeltaT* objective which means a inverse and strong relationship, instead *Delta* = 100% for the *DeltaP* and *Surface* objectives which means a very reliable and strong correlation. These is the reason why the total lenght is the most influential parameter,

but also the most inconvenient because it easily causes unfeasible designs, that exceed the constraints.

The final result of a multi-objective optimization is a set of 80 different designs belonging to the Pareto frontier, that is the set of non-dominated optimal solutions, which is shown in the bubble chart of Fig.4.7. This is a recent and innovative method integrated in *modeFRONTIER* to visualize four-dimensional data projected onto a more comprehensive two-dimensional chart, in which the two axes represent two objectives (in this case pressure drop and total heat transfer surface), while the bubble colour and diameter indicate respectively the heat transfer objective and the design *ID* number. Thus, it is easy to visualize the imaginary Pareto border given by the three objectives and the "evolution" of the designs during the optimization, in other words, how the *ID*s of the new designs "grow up" into the objectives space. Another interesting remark given from this chart, is the discontinuous distribution of the designs: this fact depends on the discretization of the cross-angle variable; the minimum step of the variation, which has been chosen equal to 0.02° for manufacturing reasons, causes as a matter of facts larges variations of the objectives. However, because of the restricted ranges of the variables, the performances of the best design selected from the Pareto frontier do not significantly improve the original *design_0*; from a quantitative point of view, values lower than 2% of improvement for each objective have been found, thus a second adjusted optimization is needed to find better designs.

(a) P1

(b) P2

(c) P3

(d) P4

(e) L_{tot}

(f) θ
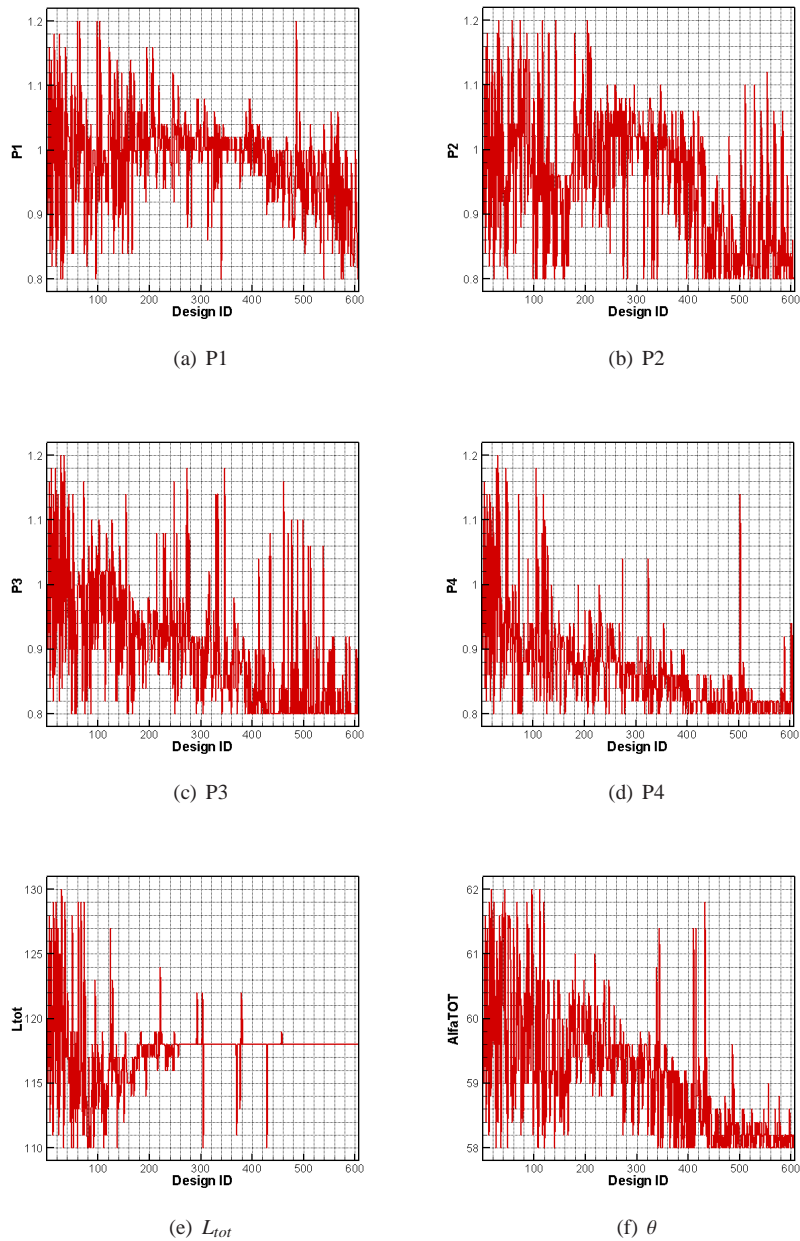
Figure 4.5 Parameters History Charts, I optimization.

(a) DeltaT

(b) DeltaP

(c) Surface
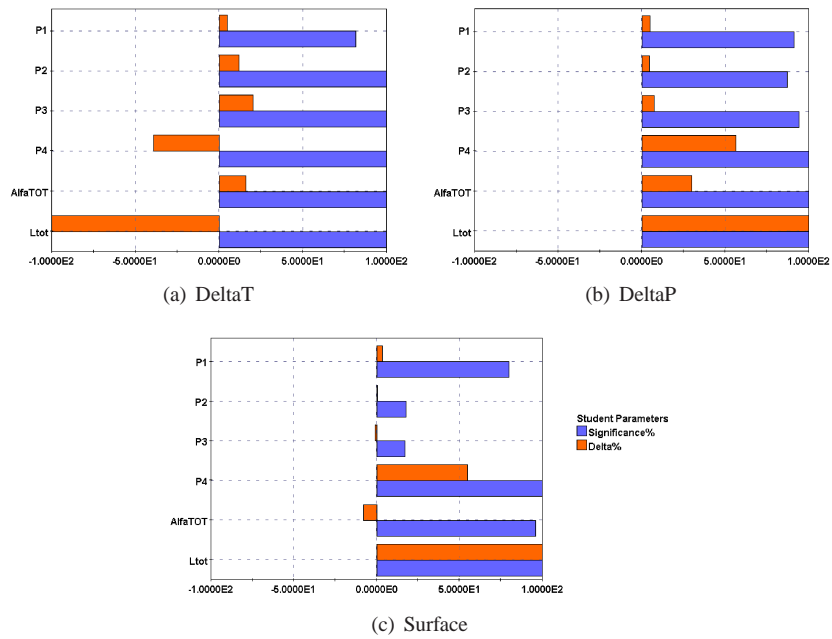
Figure 4.6 T-Student Charts, I optimization.
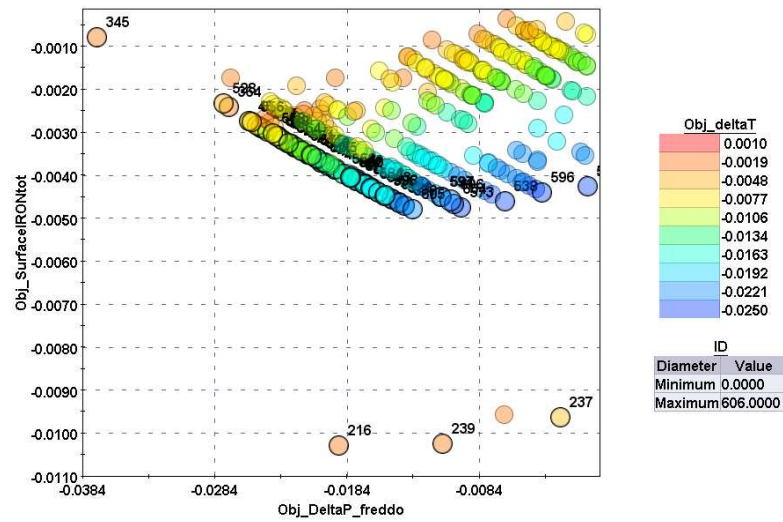
Figure 4.7 Pareto Frontier graph: encircled in black the solutions belonging to the Pareto Frontier.

Variable Name	Min Value	Max Value
$P1$	0.2	0.8
$P2$	0.2	0.8
$P3$	0.2	0.8
$P4$	0.2	0.8
$Ltot$	$118mm$	$118mm$
θ	$40°$	$60°$

Table 4.3 New variables range, second optimization.

4.6.2 Secondary Optimization

Starting from the considerations obtained by the first optimization, a second one has been performed. The main changes concern both the variables and the objectives. New ranges of the $P1$, $P2$, $P3$, $P4$ and θ variables have been modified as indicated in Tab.4.3, a constant value of L_{tot} equal to 118 *mm* has been fixed, and the analysis on only two objective functions, that are the minimization of pressure drop and minimization of total heat tranfer surface, have been focused. The third objective, that was the minimization of the temperature difference, has not been adopted, to help the optimization algorithm to converge and find better results. The reason of this choice depends on the fact that the objectives have opposite trends as indicated in the previous $t-$student charts, so the algorithm, trying to optimize each objective, leads to geometries not too far from the original one, to not break the constraints. The most important thing is that however we don't want to loose in performances, so a constraint for the heat transfer has been set up, to guarantee that the new designs have thermal performances at least equal to the best value reached in the first optimization (nevertheless better that the original *design_0*).

As initial design of experiments for the second multi-objective optimization, 20 different solutions inside the Pareto Frontier of the previous optimization have been chosen to start from almost good designs. The optimization has been terminated after 17 generation which means 340 total configurations calculated. The convergence history charts of the variables and the objective functions are shown respectively in Figs.4.8, 4.9.

From Figs.4.9 (a), (b) it is possible to notice how the optimization algorithm works well, minimizing both objectives. Also in this case it is possible to observe the two behaviors as in the first optimization phase; at the beginning the algorithm reaches the best region as compromise between the objectives, while in the second one there is a

	P1	**P2**	**P3**	**P4**	θ[**deg**]	**ΔP%**	**Surf**%	**ΔT%**
Des.0	1	1	1	1	60	0	0	0
Des.134	0.03	0.02	0.03	0.02	42	-19.36	-1.98	-0.28
Des.337	0.06	0.03	0.25	0.02	42	-19.64	-1.88	-0.08

Table 4.4 Details of the two best designs compared to the original one.

refinement in order to get the best designs.

The final result of the optimization (the Pareto frontier) is visible in Fig.4.10. The set is composed by 7 designs, that are the best compromise between the surface (in other words the cost of the material needed to fabricate the recuperator) and pressure drop objectives. For the choice of the final design inside the Pareto Frontier, there is the possibility to use different methods as the *Multi Criteria Decision Making* algorithms (*MCDM*) [32] in case of very complicated analyses, with a high number of objectives.

In this case, since there are only two objectives, a direct engineering approach has been adopted, where the designer directly chooses the best design, according to his preferences.

Among the 7 designs that belong to the Pareto front, two extreme designs (ID 134 and ID 337) have been analyzed and compared (as reported in Tab.4.4) to understand which of the two geometries has better performances. The design 134 has a surface area lower than 1.98% compared to the original *design*_0 and it minimize the pressure drop less than 19.36% , maintaining a lower value of the ΔT objective (-0.28%).

The other design, with ID 337, has better fluid-dynamics performance with the lowest value of ΔP, 19.64% less than the original, but just 1.44% less compared with the design 134. So in terms of differential increment in goodness it is not significant because design 337 has a surface area 1.88% lower than the original, but 5% higher than the design 134. For this reasons design 134 has been chosen as the best compromise design between the objectives.

This new optimized geometry has a sharper shape of the primary surfaces, given by the small value of *P1*, *P2*, *P3* and *P4*, and a lower value of the corrugation angle $\theta = 42°$, which means a minor number of unit cells across the length of the recuperator due to the major length of the repeating module. The comparison between the original geometry and the optimized one are given in Fig.4.12.

In Figs.4.11, where the heat flux contours on the wall for the hot domain are shown, it is possible to notice that the peaks at the points where the flow first impinges on the wall and then deviates to follow the channel are almost the same. In

fact the thermic-behavior is maintained constant due to the constraints setup in the optimization process.

From a purely fluid-dynamics point of view, in Figs.4.16, 4.17 it is possible to observe the two streams that tend to mix causing a vortex effect which enhances the heat transfer of the cross corrugated channel. Thanks to the sharpness of the surfaces, the optimized geometry induces a greater separation and so a recirculation downstream the edges. Moreover, it can be noticed from the velocity contours plotted on the cross section I in Fig.4.15, that the best design has a more uniform distribution with lower peak values. The opposite behaviour happens at the section II, Fig.4.14, in fact higher values of velocity occour where the flow meets the wall.

These results have been duly verified by running grid independence tests at several grid resolutions, up to 5×10^5 cells for each design belonging to the Pareto set as reported in Fig.4.18, where it can be seen that the global trend of the ΔP objective is maintained constant already for low number of elements, which means that at least it could be theoretically possible to run faster optimizations using coarser meshes and refining them just in a successive phase.

	Nx	Ny	Cells	DeltaP	DeltaT
	26	16	82500	100,705	97,496
	31	21	154800	100,295	99,132
Orig. Des.	36	26	259700	100,117	99,860
	46	26	403200	100,024	99,971
	51	26	510300	100,000	100,000
	26	16	82500	80,573	98,131
	31	21	154800	80,958	98,846
Opt. Des.	36	26	259700	81,121	99,181
	41	31	403200	81,195	99,356
	46	31	510300	81,186	99,367

Table 4.5 Tables of values during the structured mesh independence.

(a) P1

(b) P2

(c) P3

(d) P4

(e) θ
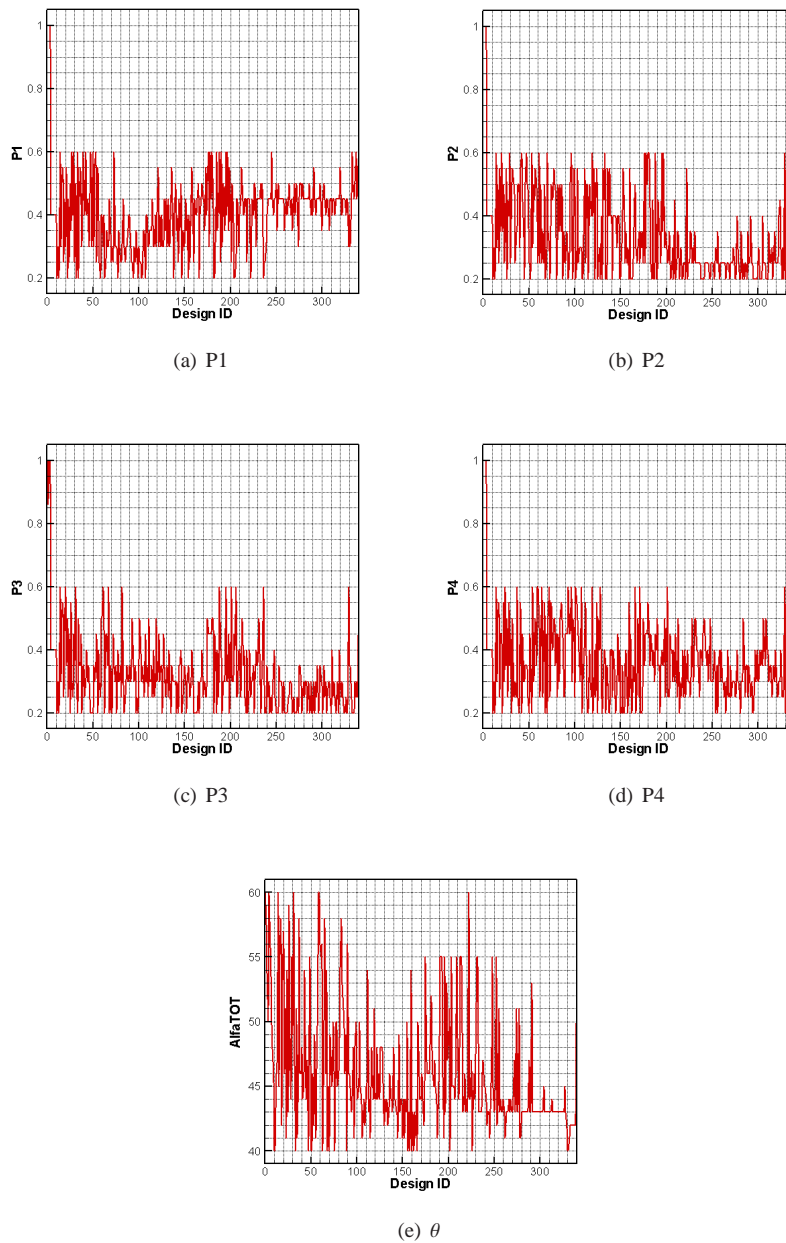
Figure 4.8 Parameters History Charts, II optimization.

(a) DeltaP

(b) Surface
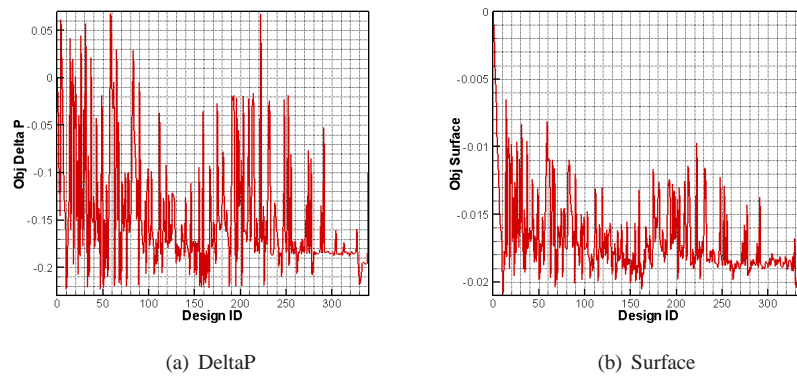
Figure 4.9 Objectives History Charts, II optimization.
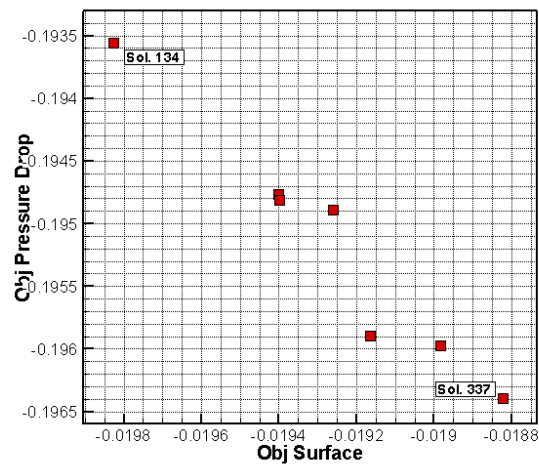
Figure 4.10 Pareto Frontier of the final optimization. The design 134 has been chosen as best configuration of the entire project.
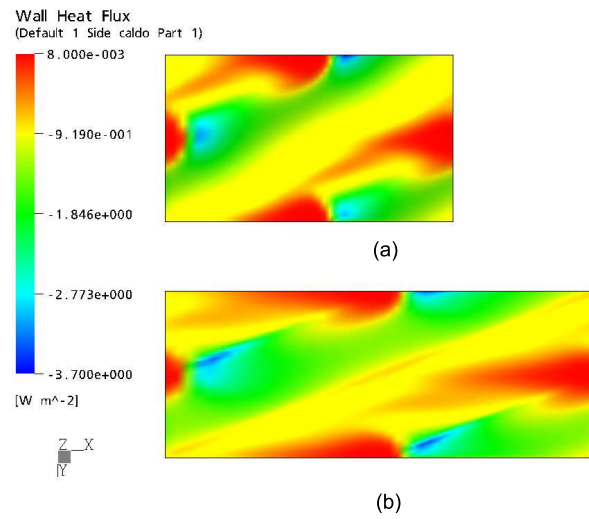
Figure 4.11 Comparison between wall heat flux.
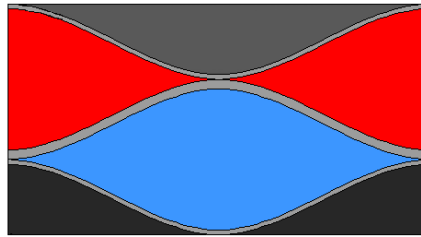
(a) Initial geometry
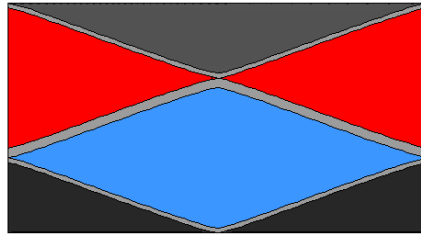
(b) Final optmized geometry

Figure 4.12 Comparison between the original and optimized geometries.
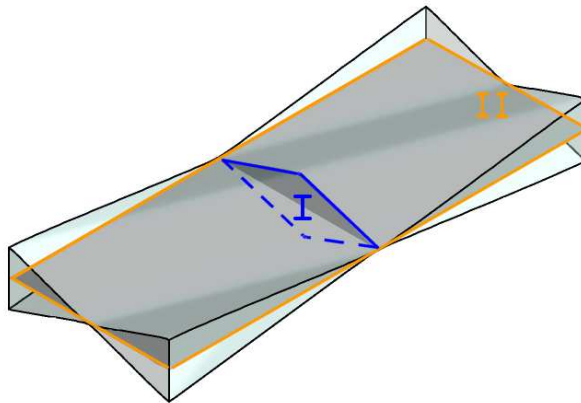
Figure 4.13 Cross sections for plot visualization.
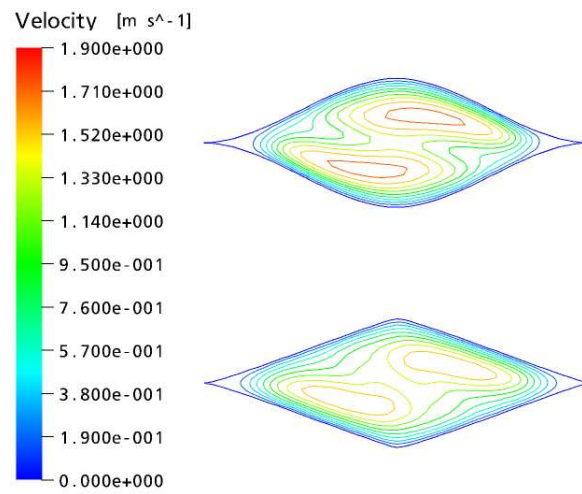
Figure 4.14   Comparison between velocity contours on cross section I.
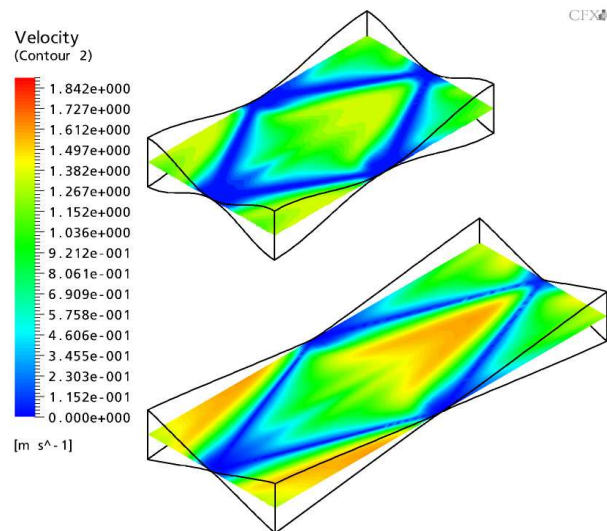
Figure 4.15   Comparison between velocity contours on section II.
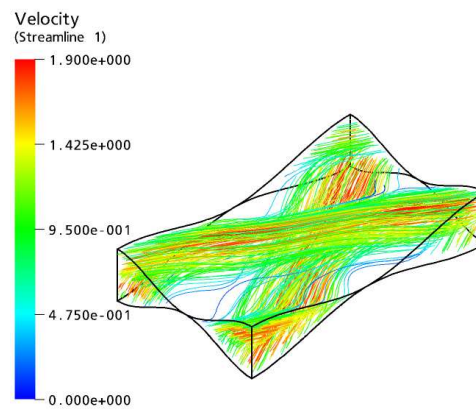
Figure 4.16 Streamlines visualization, original geometry, *design0*.
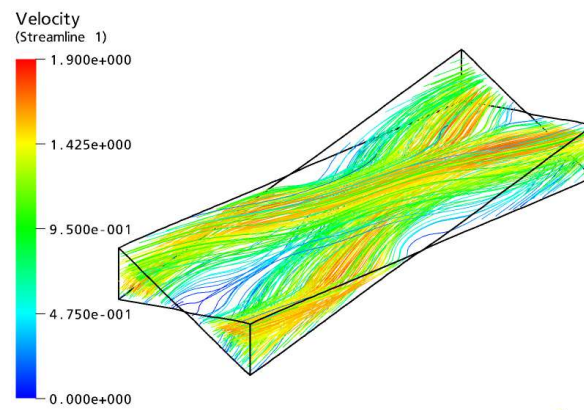
Figure 4.17 Streamlines visualization, optimized geometry, *design134*.
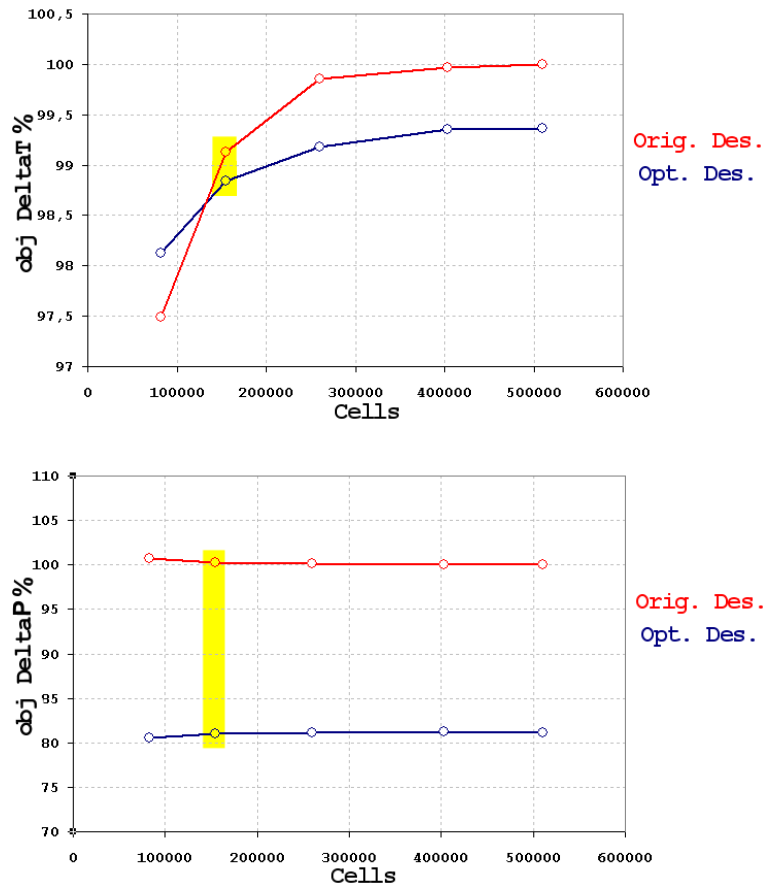
Figure 4.18   Comparison of grid independence.

4.7 New methodologies

In this section the brief description of two novel applications in turbomachinery fields is presented, in order to show which would be the future techniques that could help the design of such devices. The first is a methodology for design of recuperators based on the optimization of the performance stability is illustrated. This technique is an alternative approach compared to the traditional one performed in the previous section, which considers just a design point and tends to "over-optimize", producing solutions that perform well at the design point but have poor off-design characteristics. This method has been initially implemented for design of airfoils in transonic field, searching for solutions that are stable in terms of performance with the fluctuations of Mach number and angle of attack [33], but it demonstrates to be a valid methodology also in turbomachinery fields.

Besides this, the second section consists in a novel application of a recent tool to visualize natural groupings and relationships in high-dimensional data is presented. This methodology called *Self-Organizing Map*, projects complex data onto a two-dimensional map preserving the topology so that similar data items will be mapped to nearby locations on the map. This method could be a help to understand the correlation between variables and objectives and could be used in coupling with the more traditional *t-student* data analyses.

4.7.1 Robust Design

The development of a design method, able to find solutions that are as more insensitive as possible to the variations of those parameters that rule the design point, is becoming more and more a requirement for industry. The name of this design method is Robust Design.

The implementation of Robust Design is interesting in many design situations; for example in preliminary design phase some parameters may be unknown and for this reason is important to find solutions as more insensitive as possible to the variation of these parameters. Other important applications can be the research of design solutions that are not sensitive to small fabrication errors or variations of the operative conditions (fluctuations of the design point). In this situations traditional optimization techniques tend to "over-optimize", producing solutions that have good performances at the design point but have poor off-design characteristics. The details of the theory and concepts behind this methodology is reported in App.A.

To follow a Robust Design approach, the designer needs to identify which are the uncontrollable variables of the process, the so-called uncertainties. Regarding gas tur-

bine, it is almost a constant volume machine at a specific rotating speed, thus the inlet air volumetric flow rate is nearly fixed regardless of the ambient air conditions. As the air temperature rises in hot summer days, its density falls but the volumetric flow rate remains constant. Therefore, the mass flow rate reduces and consequently the power output decreases [34]. In [35], a model to study the effect of inlet air-cooling on gas turbines power and efficiency is developed for hot and humid climate areas (Jeddah, Saudi Arabia); their obtained results show that the power and efficiency improvements are functions of the ambient conditions. The performance improvement is calculated for, ambient temperatures from 30 to 50°C and the whole range of humidity ratio (10ˇ100%).

By these considerations is obvious that the physical properties of the air vary due to the athmosferic condition, the longitude/latitude and altitude (Fig.4.19), and the period of the year (as shown in the chart of air density measured during the year, Fig.4.20 [36]) . So it is possible to affirm that air properties can be considered as uncertainties because they changes in sthocastic way. Nevertheless, density and dynamic viscosity are correlated by the Reynolds number, so it can be assumed that a good way to impose a fluid-dynamics uncertainty of the problem, consists in varying the Reynolds number into a restricted operating range given by the maximum variations of air properties during the year. Obviously, the same reasoning could be carried out on thermal aspects, such as how geografical variables could influence the air specific heat or thermal conductivity. However, given that within this method, the number of objectives doubles because both mean value and standard deviation are considered, just the Reynolds number has been perturbed in order to demonstrate that this methodology can be applied to the design of microgas turbine recuperators. To increase the optimization process, the Robust Design approach has been coupled with the *Game Theory* algorithm, whose details are given in App.B, which has demonstrated to be better in managing problems with a high number of objectives, and faster than the Genetic Algorithm in spite of slight lower accuracy of the results [37]. The good performance shown by the coupling of these two methodologies has been proved in the design of hydraulic turbines [38].

The results of the new optimization, which has been terminated after 240 designs, give that the new robust designs found in the second optimization, whose details are reported in Tab.4.6, have better performances in term of both mean values and standard deviation, in comparison with the original *design*_0. However they do not have the same absolute good performances of *design*_134, which is the best design found with the traditional non-robust approach. In other words, the peaks of the objective values have been limitated by the algorithm during the optimization in order to find designs with higher stability, when varying the Reynolds number.
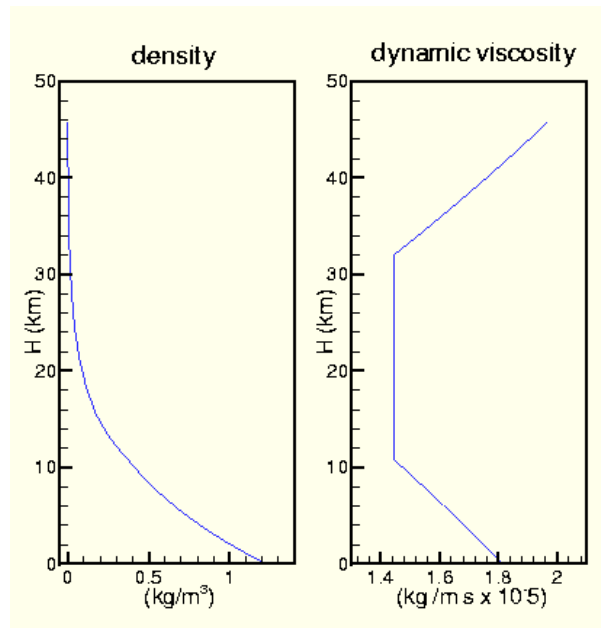
Figure 4.19 Variation of the air properies on function of altitude.
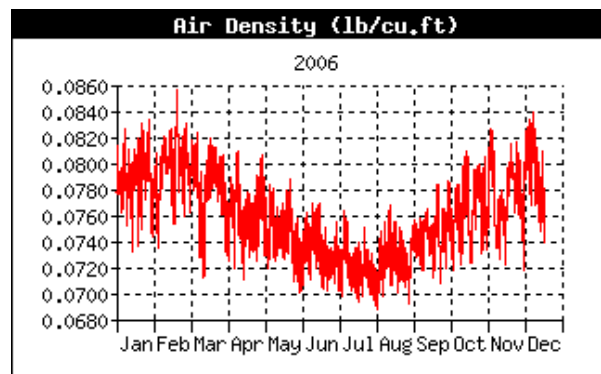
Figure 4.20 Variation of the air density during the year.

Id	P1	P2	P3	P4	θ
189	0.4	0.48	0.36	0.21	41.6
144	0.2	0.2	0.26	0.2	41.4
179	0.22	0.5	0.28	0.25	41.8

Table 4.6 Geometric parameters of the 3 best designs, Robust Design optimization.

Id	Surface	DeltaP:M	DeltaP:SD	DeltaT:M	DeltaT:SD
189	−1.88%	−17.45	−11.69	−0.12	−58.19
144	−2.04%	−14.13	−19.98	−0.65	−30.50
179	−1.92%	−14.88	−26.27	−0.47	−56.27

Table 4.7 Objective values of the 3 best designs, Robust Design optimization.

4.7.2 Self-Organizing Map

The Self-Organizing Map (SOM)[31] is an unsupervised neural network algorithm that projects high-dimensional data onto a two-dimensional map. The projection preserves the topology of the data so that similar data items will be mapped to nearby locations on the map. This allows the user to identify "clusters", i.e. large groupings of a certain type of input pattern. Further examination may then reveal what features the members of a cluster have in common. The maps comprehensively visualize natural groupings and relationships in the data and have been successfully applied in a broad spectrum of research areas ranging from speech recognition to financial analysis. The details of the theory of this methodology is reported in App.C.

By running the Self-Organizing Map on the values of the objectives of the primary optimization, it is possible to visualize in Fig.4.21 the direct correlation between *DeltaP* and *Surface* and the inverse relationship between *DeltaT* and the other two objectives. The whole of the designs could be grouped in three main clusters, subdivided by the black edges, as follows:

- The upper right corner corresponds to the designs with high bulk temperature difference of the fluids, and low primary surfaces and pressre drop.

- The upper left corner correspond to the opposite of the upper right one.

- The rest of the domain has average values of objective functions.

Comparing the objective maps with the maps colored by the geometric parameters in Fig.4.22, it is possible to notice the close correlation between L_{tot} and the objectives, and instead the absence of correlation with the other variables; this is probably due to the extremely strict ranges of these parameter, which has been the main reason that leads to the realization of the second optimization.

The maps obtained utilizing the results of the second optimization are shown in Figs.4.24, 4.23. A clear correlation between the map of θ with the maps of *DeltaP* and *Surface* is visible, which was impossible to notice in the first optimization. The main reason could be the fact that, forbidding the variation of the total lenght of the recuperator (L_{tot}), the most influential parameter became the cross-angle. Moreover, increasing the ranges of the other parameters leads to brand-new correlations; similar patterns could be noticed comparing $P3$ and $P4$ and the two objectives.

In summarize, the Self-Organizing Maps of the datas obtained with the second optimization gives that low values of θ, $P3$ and $P4$ lead to geometeries with good performances, i.e. low pressure drop and small surface.

Thus it is clear that the use of Self-Organizing Maps may complete the information extracted by the *t-student* parameter, thus helping the engineers in the design process.
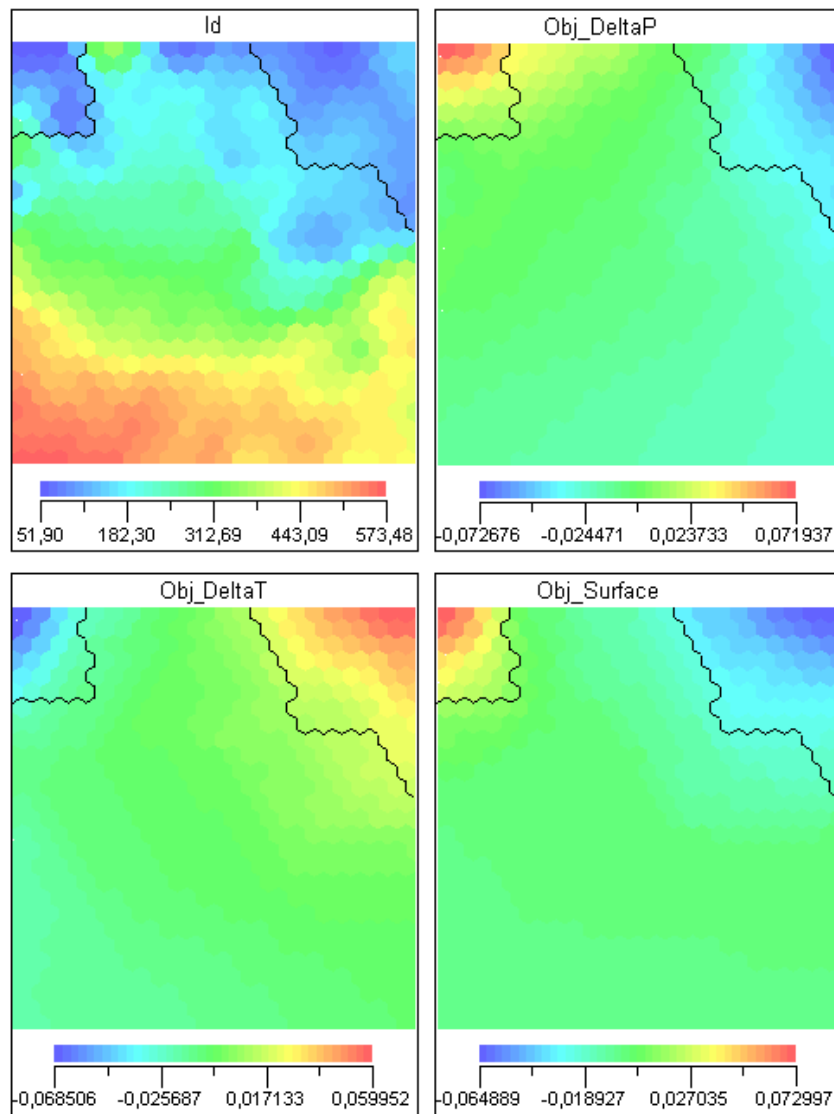
Figure 4.21 Maps of the objectives, primary optimization.
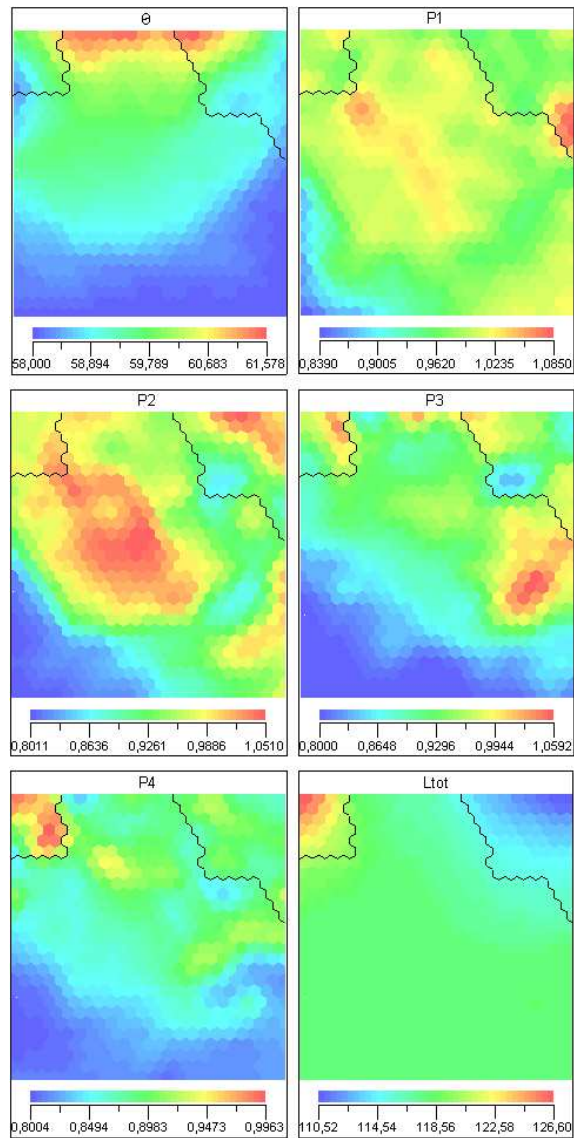
Figure 4.22   Maps of the variables, primary optimization.
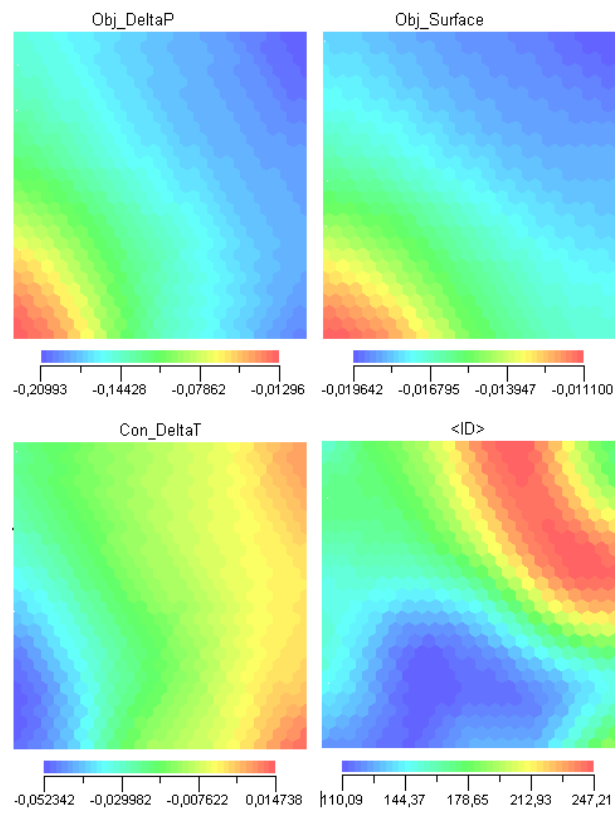
Figure 4.23 Maps of the objectives, second optimization.
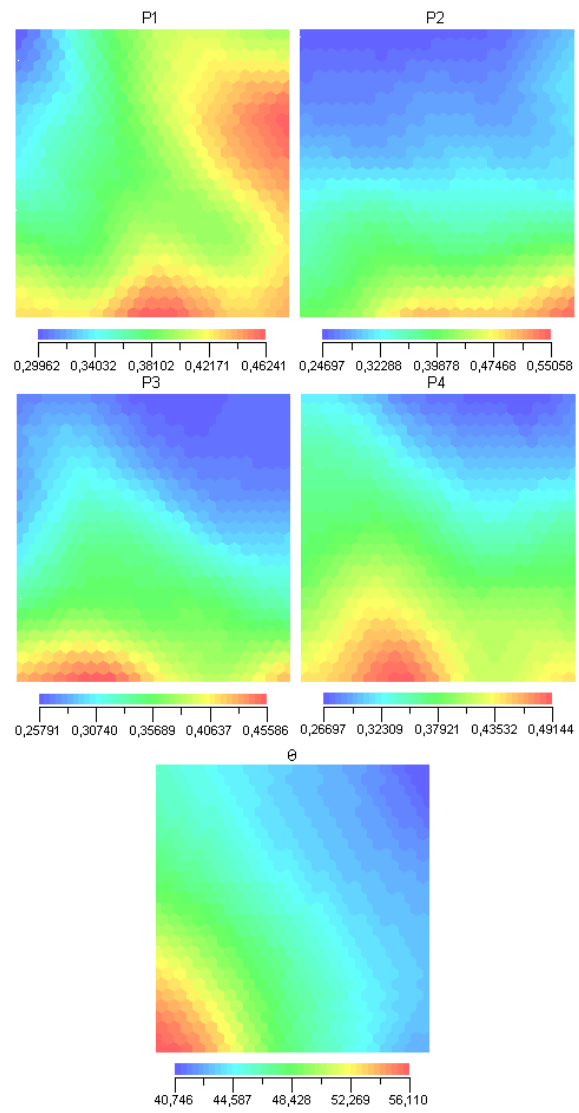
Figure 4.24 Maps of the variables, second optimization.

Conclusions

Within this thesis, a multi-objective optimization of the geometry of a microgas turbine recuperator has been presented, based on the implementation of a novel methodology that supports the application of numerical simulation and optimization techniques in engineering design.

One of the activities of this work was the integration of a set of computer-aided engineering tools in order to calculate both the thermal and hydraulic properties of the device. An industrial parametric CAD tool has been utilized to carry out the parameterization of the shapes of the heat transfer surfaces, which allows an easy and automatic variation of the geometry and the resulting computational grid.

The numerical simulations of this recuperator have been carried out considering a single periodic module, due to the repetitive pattern of the behavior in fully developed flows. Moreover, the analyzed geometry comprises both hot and cold fluid streams and the solid layers between them, avoiding the necessity of imposing artificial constant-temperature or constant-flux boundary conditions. This numerical model has been successfully implemented into a commercial CFD tool and then validated by comparison with literature data.

Optimizations have been then conducted based on the outcome of these simulations by means of a process integration environment, capable to manage the integration of several industrial packages and to solve the optimization problem adopting, among other algorithms, the Multi Objective Genetic Algorithm and the Game Theory.

A final optimal geometry of compact recuperator has been found, which differs remarkably from the usual geometries reported in literature. It improves all the objectives, in particular pressure drop and, more slightly, cost, without any penalty in wall heat flux. It must be noted that such results have been obtained with constant hydraulic diameter and, consequently, constant mean flow velocity and Reynolds number. The values of these parameters were chosen according to best practice design rules.

The numerical results of the optimized geometry have been validated managing a comparative grid independence in relationship with the results of the original geometry. The difference between the values is maintained during the mesh refinement process so an effective errorless improvement of the performances has been reached.

In the last phase of the work, a different optimization approach has been implemented taking into account the variability of the design point. A probabilistic definition of the boundary conditions has been adopted, and the design problem has been solved by means of a Robust Design Optimization methodology. Besides, a complete statistical analysis of the result have been conducted by means of the most recent techniques, in order to find possible correlation between variables and objectives.

The described procedure could be applied not only to the design of microgas turbine recuperators, but in principle, to even more complex design problems.

Appendix A

Robust Design

In many industrial applications, some values of the input design parameters are not known. For example, uncertainties could characterize some geometric entities (lengths, relative positions, angles ...) correlated to the problem in exam. Many times the operative conditions are not fixed but there is the presence of fluctuations: in turbo-machinery the mass flow rate, the inlet pressure, or in aeronautic, the flight speed, the angle of attack, the air temperature, etc. For these reasons many input parameters are known by the mean value and the variance, and the gaussian theory is used to define the stability of the solution under the uncertainties of the input parameters.
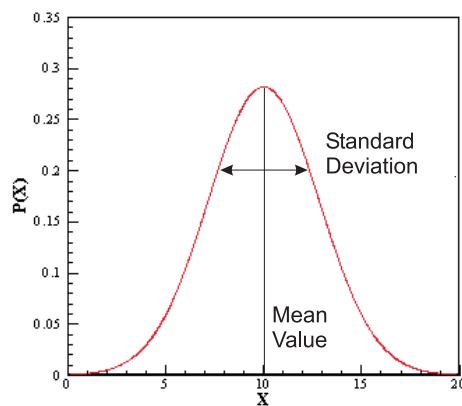
Figure A.1 Gaussian distribution of input parameter.

When there is the presence of fluctuations in the operative conditions, it is important to define the stability of solution because a traditional optimization approach

could tend to "over-optimize" (Fig.A.2), giving high performances solutions corresponding to the design point but with poor off-design characteristics.
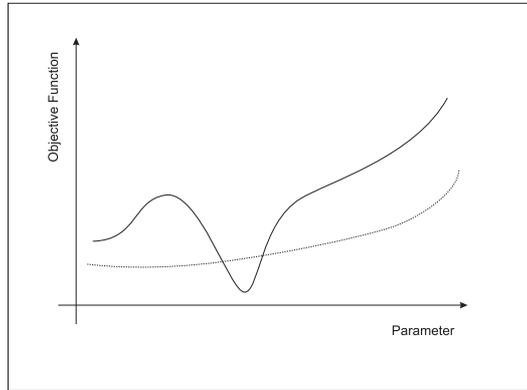
Figure A.2 Comparison between a single design point optimization and Robust Design approach.

Many numerical methods have been developed to optimize the design under uncertainty of the input parameters : [39], [40], [41], [42].

The method [40] is not deeply related to optimization field; it identifies designs that minimize the variability of the performance under uncertain operating conditions, so it is a procedure a posteriori; [39] uses an optimization method developed from a multi point approach; for the drag reduction of an airfoil, the objective function is:

$$\min \sum_{i=1}^{n} \omega_i C_d(d, \alpha, M_i) \tag{A.1}$$

where ω_i are arbitrary weights, d is a set of airfoil geometric design variables and c_d is the drag coefficient. The problem of this formulation is that the result of the optimization depends on the difficult choice of the weights ω_i.

In [42] a new optimization method has been shown, based on the definition of a performance function, defined in the entire space of the fluctuation conditions; for the same case of [39]:

$$\min \int_M C_d(d, \alpha, M) f_M(M) dM \tag{A.2}$$

where $f_M(M)$ is the probability density function which, in this case, depends only on the Mach number. The method used in [42] shows that it is possible to find a more stable airfoil, referred to drag coefficients, when there are fluctuations in the Mach number.

In that previous works it is possible to observe that a mono objective approach has been used, where the performance (c_d) and the stability (weights w_i and probability density function $f_M(M)$) are joined in an unique objective function. For this reason after the optimization phase, the designer can get only one solution, without choice between different designs with different performance and stability.

In this thesis, a recent method for a Robust Design optimization is shown. The main idea is to use a multi objective approach to reach the best compromise between performance and stability of the design. With reference to Fig.A.3, it is possible to notice that the function has an absolute extreme (x_1) and a relative extreme (x_2); in this case the uncertainties could be represented by the tolerance δ of the input parameter x. Obviously a standard optimization, without considering fluctuations, would find out the point x_1. With a Robust Design optimization (presence of tolerance δ) two different objectives have to be considered: mean performance and stability of the solution. Considering the mean performance, the best configuration would be represented by the point x_1, since the mean value of the function is the highest inside the tolerance δ. For the stability the best configuration is represented by the point x_2, because the function is characterized by a lower variability.

Consequently it is interesting to observe that when a Robust Design optimization is performed, it is possible that the more stable region doesn't correspond to the more performing one. So, to run an optimization under fluctuations, the best way is to define two different objectives for every function to optimize: the mean value of the function and the variance of the same function. In mathematical terms:

$$\max \ E(f) = \int_q f(x,q)p(q)dq \tag{A.3}$$

$$\min \ \sigma^2(f) = \int_q (f(x,q) - E(f))^2 p(q)dq \tag{A.4}$$

where f is the function to maximize according to Robust Design concept, q are uncertain parameters, modelled by probability density function $p(q)$.

Dealing with engineering problems it is hard to adopt continue formulations. So the problem of an optimization under uncertainties becomes a Multi Objective Optimization problem where the objectives are performance (Eq.A.3) and stability (Eq.A.4). As optimization algorithm a Multi Objective Genetic Algorithm (MOGA)
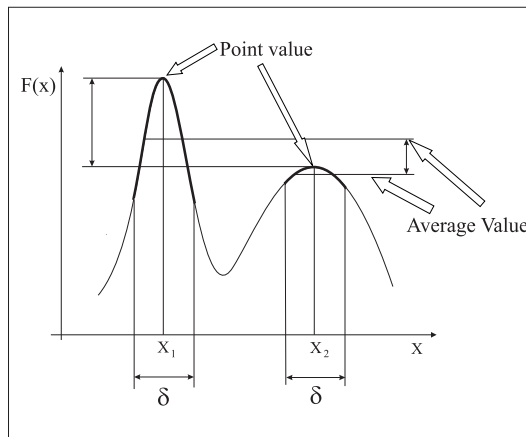
Figure A.3   Function with 2 extremes: not stable absolute maximum x_1, stable relative maximum x_2.

has been adopted because this is the best methodology [43], [44] to solve a real multi objective problem without using a weighted function as:

$$\max \ f_w = \omega_1 \bar{f} + \omega_2 \sigma_f \tag{A.5}$$

in fact it is tricky to know the exact values of the weights w_i, and this is the reason by which it should be better refer to the MOGA approach.

It is interesting to note that after the optimization phase, the designer doesn't get only one solution [42] but a set of solutions (Pareto Front) that represents the best possible compromise between the different objectives. An example of a Pareto Front for a Robust Design Optimization could be observed in Fig.A.4; inside the Pareto Front it is possible to choose different compromises between performance and stability, with more flexibility than a standard optimization, where the solution is unique without choice between the objectives.

It is important to underline that is possible to face a wide range of problems with the Robust Design approach such as small manufacturing process errors, fluctuations in the operative conditions, unknown input parameters, etc.
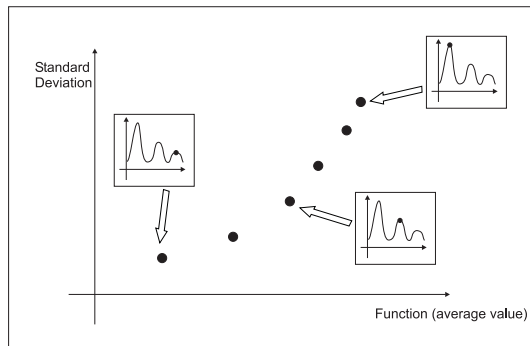
Figure A.4 Pareto Front in a Robust Design Multi Objective Optimization.

Appendix B

Game Theory

The Multi Objective Game Theory methodology is based on the competitive game theory proposed by Nash. The objectives and the variables of the optimization problem are decomposed among the players that, through the application of a defined number of Simplex iterations, try to optimize their own objective function, influencing each other by the sharing of the best variables obtained after each step of the game as explained in [37]. The number of players equals the number of objectives. It is to be underlined that this optimization scheduler combines the fast convergence speed of Simplex with the multi-objective strategy, introduced by Nash's competitive game theory.

In a competitive game, the players act following different objectives. For example, in a two-objective optimization, player A have to choose his strategies in order to minimize his function f_A, while player B have to minimize the function f_B. In other words, each player is forced to optimize his variables following his objective, but it is constrained by the value of the variables that have been found at the end of each step by the other players, and that become fixed during his search. The aim of a competitive game is to find a Nash equilibrium point which is defined in mathematical terms as $(x^*, y^*) \in A \times B$ if and only if:

$$\begin{cases} f_A(x^*, y^*) = inf\ f_A(x, y^*) & x \in A \\ f_B(x^*, y^*) = inf\ f_B(x^*, y) & y \in B \end{cases} \tag{B.1}$$

Of course, as generally both the functions depend on the two domains, the strategies of one player influences the choices of the other one: the two players act simultaneously until an equilibrium is found: in that case, each player has minimized his own function with a common pair of strategies.

The initial decomposition of variables and objectives is random but, in the following steps, it is changed accordingly to statistical analysis: using it and in particular the *t-Student* coefficient it is possible to decide, at the end of each player step (that is after a certain number of Simplex iterations), if a variable is statistically significant for the

player to which it was assigned or not and, in the latter case, i.e. if the significance percentage is lower than an assigned threshold, the variable is given to another player in the following step. In other words, the significance percentage expresses the probability that a variation of the objective function is really produced by a variation of the variables belonging to the same player instead of an effect of the statistical variance around the mean value of the objective function.

For each variable the *t-Student* value is determined from the database of designs calculated for each player. This statistical parameter substantially expresses the difference of the mean values of fitness calculated from the data characterized by a high value of the variable ([0.5-1] half of the range, x_1) and by a low value ([0-0.5] half of the range, x_2), divided by the standard deviation of the data with reference to the mean values:

$$t = \frac{|\overline{x_1} - \overline{x_2}|}{\sigma} \tag{B.2}$$

in which the standard deviation σ is expressed as:

$$\sigma = \sqrt{\frac{\left(\sum_{i=1}^{n_1}(x_{1i} - \overline{x_1})^2 + \sum_{i=1}^{n_2}(x_{2i} - \overline{x_2})^2\right) \cdot (n_1 + n_2)}{(n_1 + n_2 - 2) \cdot n_1 \cdot n_2}}. \tag{B.3}$$

After a certain number of Simplex iterations that is defined by the user, each player finds the best configuration (and set of variables) for its objective, and then the search continues with a new step, in which the variables that are fixed for each player are updated to the values found by the other player in the previous step.

The game continues for a defined number of steps or until the "Nash equilibrium point" is found. In the latter case, each player have completely optimized his objective, thus the variables values found by each player represent the best compromise of all the competitive objectives.

Appendix C

Self-Organizing Map

The Self-Organizing Map belongs to the class of unsupervised and competitive learning algorithms. It is a sheet-like neural network, with nodes arranged as a regular, usually two-dimensional grid. Each node is directly associated with a weight vector. The items in the input data set are assumed to be in a vector format. If n is the dimension of the input space, then every node on the map grid holds an n-dimensional vector of weights. The basic principle is to adjust these weight vectors until the map represents "a picture" of the input data set. Since the number of map nodes is usually significantly smaller than the number of items in the dataset, it is needless to say that it is impossible to represent every input item from the data space on the map. Rather, the objective is to achieve a configuration in which the distribution of the data is reflected and the most important metric relationships are preserved. In particular, interest is in obtaining a correlation between the similarity of items in the dataset and the distance of their most alike representatives on the map. In other words, items that are similar in the input space should map to nearby nodes on the grid.

The algorithm

The algorithm proceeds iteratively, so on each training step a data sample **x** from the input space is selected. The learning process is competitive, meaning that a winning unit c on the map is determined, whose weight vector **m** is most similar to the input sample **x**.

$$\|x - m_c\| = min_i \|x - m_i\| \tag{C.1}$$

The weight vector m_c of the best matching unit is modified to match the sample **x** even closer. As an extension to standard competitive learning, the nodes surrounding the best matching unit are adapted as well. Their weight vectors m_i are also "moved towards" the sample **x**. The update rule may be formulated as:

$$m_i(t + 1) = m_i(t) + h_{ci} * (x - m_i(t)) \tag{C.2}$$

The scalar factor $h_{ci}(t)$ is often referred to as the "neighbourhood function". It is usually a Gaussian curve, decreasing from the neighbourhood centre node c to the outer limits of the neighbourhood.

$$h_{ci}(t) = \alpha(t) * exp\left(-\frac{\|r_c - r_i\|^2}{2\sigma(t)^2}\right) \tag{C.3}$$

In the above equation, $\alpha(t)$ is another scalar multiplier called the "learning rate" which may be regarded as the height of the neighbourhood kernel. $\sigma(t)$ is the radius or the width of the neighbourhood kernel. It specifies the "region of influence" that the input sample has on the map. Both the height and the width of the neighbourhood function decrease monotonically with time. As can be seen, nodes closer to the best matching unit will be more strongly adjusted than nodes further away. At the beginning of the learning process, the best matching unit (BMU) will be modified very strongly and the neighbourhood is fairly large. Towards the end, only very slight modifications will take place and the neighbourhood includes little more than the BMU itself. This corresponds to "rough ordering" at the beginning of the training phase and "fine" tuning near the end. Since not only the winning node is tuned towards the input pattern but also the neighbouring nodes, it is probable that similar input patterns in future training cycles will find their best matching weight vector at nearby nodes on the map. In the run of the learning process, this leads to a spatial arrangement of the input patterns, thus inherently clustering the data. The more similar two patterns are, the closer their best matching units are likely to be on the final map. It is often said, that the Self-Organizing Map folds like an elastic net onto the "cloud" formed by the input data. It is important to state that the Self-Organizing Map algorithm is not a clustering algorithm. It is intended primarily as a tool to reduce the dimensionality of the data and for information visualization. Of course, this includes the visualization of groups of similar items. But the Self-Organizing Map is not a tool that will produce an explicit partitioning of a dataset into a precise number of groups. This also explains why the concept of a "cluster" is not well defined for the Self-Organizing Map. The maps do not show sharp cluster borders and there is no obvious centroid. Of course, one can theoretically think of each node on the map as a cluster centroid. The cluster corresponding to each node could then be said to include all dataset items mapping to this node. But this is not a sound approach in the practical application of the *SOM*. It tempts the user to use small maps of only k nodes, expecting that this will produce k clusters in the same way k-means does. The

results with such small maps, however, are very poor. The heart of the algorithm is the neighbourhood function and the concept of adjusting not only the best matching unit but also its surrounding units. This will create "neighbourhoods" of similar nodes, but only if the space on the map is sufficiently large to allow this. An interesting point regarding the topological preservation is that this refers not only to the intra-cluster relationships but also to the inter-cluster relationships, in other words, not only the distances of objects within a cluster are meaningful, but also the distances between clusters.

Acknowledgments

Bibliography

[1] Stasiek J. Collins M. W. Ciofalo M. Investigation of flow and heat transfer in corrugated passages - i. experimental results. *Int. J. Heat Mass Transfer*, 39(1):149:164, 1996.

[2] Chiang H.D.Wang C. Hsu C. Performance testing of a microturbine generator set with twin rotating disk regenerators. *Proceedings of ASME TurboExpo 2004, June 14-17, 2004, Vienna, Austria*, 2004.

[3] Wilson D.G. Regenerative heat exchangers for microturbines, and an improved type. *Proceedings of ASME TurboExpo 2003, June 16-19, 2003, Atlanta (USA)*, 2003.

[4] Lagerstrom G. Xie M. High performance & cost effective recuperator for micro-gas turbines. *Proceedings of ASME TurboExpo 2002, June 3-6, 2002, Amsterdam, The Netherlands*, 2002.

[5] Curzio E.L. Maziasz P.J. Pint B.A. Test facility for screening and evaluating candidate materials for advanced microturbine recuperators. *Proceedings of ASME TurboExpo 2002, June 3-6, 2002, Amsterdam, The Netherlands*, 2002.

[6] Maziasz P.J. Swindeman R.W. Selecting and developing advanced alloys for creep-resistance for microturbine recuperator applications. *Proceedings of ASME TurboExpo 2001, June 4-7, 2001, New Orleans, Louisiana (USA)*, 2001.

[7] Rakowski J.M. Stinner C.P. Lipschutz M. Montagne J.P. The use and performance of oxidation and creep resistent stainless steels in exhaust gas primary surface recuperator application. *Proceedings of ASME TurboExpo 2004, June 14-17, 2004, Vienna, Austria*, 2004.

[8] McDonald C.F. Low cost recuperator concept for microturbine applications. *Proceedings of ASME TurboExpo 2000, May 8-11, 2000, Munich, Germany*, 2000.

[9] Kesseli S. Wolf T. Nash J. Freedman S. Micro, industrial and advanced gas turbines employing recuperators. *Proceedings of ASME TurboExpo 2003, June 16-19, 2003, Atlanta (USA)*, 2003.

[10] Traverso A. Zanzarsi F. Massardo A. Cheope: a tool for the optimal design of compact recuperators. *Proceedings of ASME TurboExpo 2004, June 14-17, 2004, Vienna, Austria*, 2004.

[11] Maziasz P.J. Pint B.A. Shingledecker J.P. More K.L. Evans N.D. Curzio E.L. Austenitic stainless steels and alloys with improved high-temperature performance for advanced microturbine recuperators. *Proceedings of ASME TurboExpo 2004, June 14-17, 2004, Vienna, Austria*, 2004.

[12] Antoine H. Prieels L. The acte spiral recuperator for gas turbine engines. *Proceedings of ASME TurboExpo 2002, June 3-6, 2002, Amsterdam, The Netherlands*, 2002.

[13] Proeschel R. Proe 90tm recuperator for microturbine applications. *Proceedings of ASME TurboExpo 2002, June 3-6, 2002, Amsterdam, The Netherlands*, 2002.

[14] Stasiek J. Experimental studies of heat transfer and fluid flow across corrugated-undulated heat exchanger surfaces. *Int. J. Heat Mass Transfer*, 41(6-7):899:914, 1998.

[15] Utriainen E. Sundèn B. A comparison of some heat transfer surfaces for small gas turbine recuperators. *Proceedings of ASME TurboExpo 2001, June 4-7, 2001, New Orleans, Louisiana (USA)*, 2001.

[16] Croce G. D'Agaro P. Numerical analysis of forced convection in plate and frame heat exchangers. *International Journal of Numerical Methods for Heat and Fluid Flow*, 12(6):756–771, 2002.

[17] Stasiek J. Collins M. W. Ciofalo M. Investigation of flow and heat transfer in corrugated passages - ii. numerical simulations. *Int. J. Heat Mass Transfer*, 39(1):165:192, 1996.

[18] Blomerius H. Mitra N.K. Numerical investigation of convective heat transfer and pressure drop in wavy ducts. *Numerical Heat Transfer*, Part A:37:54, 2000.

[19] Gossard D.C Zuffante R.P. Sakurai H. Representing dimensions, tolerances, and features in mcae systems. *0272-1716/88/0300-0051$01.00 1988 IEEE*, page 51:59, 1988.

[20] Zhaohua G. Shungang H. Zongying O. Pro/engineer feature modeling and application. *Engineering Design CAD & Intelligent Architecture*, 8:52:54, 1999.

[21] Lin V.C. Gossard D.C. Light R.A. Variational geometry in computer-aided design. *Computer Graphics (ACM)*, 15:171:177, 1981.

[22] Monedero J. Parametric design: a review and some experiences. *Automation in Construction*, 9:369:377, 2000.

[23] Patankar S.V. Liu C.H. Sparrow E.M. Fully developed flow and heat transfer in ducts having streamwise-periodic variations of cross-sectional area. *Transactions of the ASME*, 99, May 1977.

[24] Nobile E. Stalio E. Direct numerical simulation of heat transfer over riblets. *International Journal of Heat and Fluid Flow*, 24:356:371, 2003.

[25] Ranganayakulu C. Seetharamu K.N. Sreevatsan K.V. The effects of longitudinal heat conduction in compact plate-fin and tube-fin heat exchangers using a finite elementh method. *International journal of heat and mass transfer*, 40:1261–1277, 1997.

[26] Pediroda V. Clarich A. Mosetti G. Poloni C. Application of evolutionary algorithms and statistical analysis in the numerical optimization of an axial compressor. *International Journal of Rotating Machinery 2005*, 2:143:151, 2005.

[27] *modeFRONTIER version 3 Documentation URL* `http://www.esteco.com`.

[28] Andersson J. *Multiobjective Optimization in Engineering Design*. Dissertation, Department of Mechanical Engineering, Linköpings Universitet, 2000/2001.

[29] Webb R.L. Performance evaluation criteria for use of enhanced heat transfer surfaces in heat exchanger design. *International Journal of Heat and Mass Transfer*, 24:715:726, 1981.

[30] Webb R.L. Eckert E.R.G. Application of rough surfaces to heat exchanger design. *International Journal of Heat and Mass Transfer*, 21:1647:1658, 1972.

[31] Bergles A.E. Bunn R.L. Junkhan G.H. Extended performance evaluation criteria for enhanced heat transfer surfaces. *Letters of Heat and Mass Transfer*, 1:113:120, 1974.

[32] Ciprian M. Clarich A. Pediroda V. Poloni C. Multi attribute design of airfoil under uncertainties by combining game theory and mcdm methods. *The 18th International Conference on Multiple Criteria Decision Making, Chania, Greece, June 19-23, 2006*, 2006.

[33] Parussini L. Pediroda V. Obayashi S. A metamodel based method for design under uncertainties in aeronautics. *JSME International Journal*, 48, 2005.

[34] Ameri M. Nabati H. Keshtgar A. Gas turbine power augmentation using fog inlet cooling system. *Proceedings ESDA04 7th Biennial Conference Engineering Systems Design and Analysis, Manchester, U.K., Paper ESDA2004-58101.*, 2004.

[35] Alhazmy M.M. Jassim R.K. Zaki G.M. Performance enhancement of gas turbines by inlet air-cooling in hot and humid climates. *International Journal of Energy Research.*, 30:777:797, 2006.

[36] *Jerusalem Weather, URL* http://www.02ws.com/station.php?lang=0.

[37] Clarich A. *Innovative parameterization techniques and optimization algorithms for the aerodynamic shape design*. Tesi di Dottorato, Università degli Studi di Udine, Facoltà di Ingegneria, 2004/2005.

[38] Nardin L. *CFD based design od hydraulic turbines using multiobjective optimization*. Tesi di Laurea, Università degli Studi di Trieste, Facoltà di Ingegneria, Dipartimento di Ingegneria Navale, del Mare e per l'Ambiente, 2004/2005.

[39] Drela M. Pros and cons of airfoil optimization; in *Frontiers of Computational Fluid Dynamics 1998. edited by D. A. Caughey and M. M. Hafez, World Scientific*, pages 363–381, 1998.

[40] Fowlkes W.Y. Creveling C.M. Engineering methods for robust product design using taguchi mehods in technology and product development. *Readin, MA:Addison-Wesley*, 1995.

[41] Huyse L. Lewis R.M. Aerodynamic shape optimization of two-dimensional airfoil under uncertain conditions. *ICASE Report 2001-1*, 2001.

[42] Padula S.L. Li W. Options for robust design optimization under uncertaintly. *AIAA Conference*, 2002.

[43] Poloni C. Pediroda V. Ga coupled with computationally expensive simulations: tool to improve efficiency. *Genetic Algoritms and Evolution Strategies in Engeneering and Computer Science, edited by Wiley Sons.*, 1997.

[44] Deb K. Multi-objective genetic algorithms: Problem difficulties and construction of test problems. *Evolutionary Computation 7 (3).*, pages 205–230, 1999.